



NTNU – Trondheim
Norwegian University of
Science and Technology

LIFE PREDICTION FOR HEAVY STRUCTURES BASED ON FATIGUE CRACK INITIATION AND GROWTH

Viggo Røneid

Product Design and Manufacturing

Submission date: June 2012

Supervisor: Gunnar Härkegård, IPM

Co-supervisor: Agnes Marie Hron, DNV
Vidar Osen, LINK

Norwegian University of Science and Technology
Department of Engineering Design and Materials

Prephase and acknowledgments

This master thesis marks the end of the two year Master of Science degree in Engineering Design and Materials at the Norwegian University of Science and Technology with specialization in structural integrity and materials, for me student Viggo Røneid.

I would like to thank those who have made this thesis possible, and those who have supported me throughout this period.

First of all I would like to thank my main supervisor Professor Gunnar Härkegård for giving me the opportunity to choose this project. I would also like to thank him for the support and guidance, not only through this thesis, but for guidance and support though the last two years. For this, I am grateful.

I would also like to thank Agnes Marie Horn and Stig Wästberg at DNV for make this thesis possible and for the support they have given me.

Vidar Osen and Dag Olav Kjellemo at LINK_{fr} deserves a thanks for much for much needed support throughout this project.

I would also like to thank Ph.D Candidate Ali Cetin, for his encouragement and support throughout the last year.

Stine Vethe my colleague for the last year, also deserves a thanks, for all the support, motivation and inspiration she has given me.

Viggo Røneid

Tondheim, 18th June 2012

description

THE NORWEGIAN UNIVERSITY
OF SCIENCE AND TECHNOLOGY
DEPARTMENT OF ENGINEERING DESIGN
AND MATERIALS

**MASTER THESIS SPRING 2012
FOR
STUD. TECHN. VIGGO RØNEID**

***LIFE PREDICTION FOR HEAVY STRUCTURES BASED ON FATIGUE CRACK
INITIATION AND GROWTH***

***Prediksjon av levetid for tunge konstruksjoner basert på initiering og tilvekst av utmat-
tingssprekker***

Fatigue is material ‘damage’ caused by a (large) number of load reversals: irreversible slip processes (generally at a free surface) lead to the initiation of cracks in the micrometre range, which subsequently grow into the millimetre range (and beyond) [1]. In fatigue design, one differentiates between stress-life (S-N) or strain-life (e-N) based methods on the one hand, and fatigue crack-growth (FCG) based methods on the other. The stress- (or strain-) life method predicts the number of cycles required for a macroscopic crack (crack size ≈ 1 mm) to ‘initiate’, whereas FCG methods predict the number of cycles required for a crack to grow from an initial depth of 0.1–1 mm, say, to a critical depth. Thus, the former methods are often applied to the fatigue assessment of forged, rolled, extruded or drawn products, in particular where ‘clean’ alloys are used, e.g., spring, bearing and tool steels, whereas FCG methods are well suited to the fatigue assessment of welded or cast products. All ‘heavy’ structures tend to exhibit crack-like defects from manufacturing or material processing in the range 0.1–1 mm [2].

In the present study, alternative methods for the fatigue life prediction of ‘heavy’ structures should be reviewed and critically assessed and recommendations should be given.

The study should consider stress-life (‘initiation’) [3] and crack-growth based methods [4–10] as well as ‘two-phase’ methods (covering initiation and growth) [11] ranging from advanced mechanism-based models to methods prescribed by codes, standards and guidelines [12].

Possible computation tools range from manual analysis to S-N based fatigue post-processors such as fe-safe™ or da/dn based fatigue assessment software such as CrackWise or P•FAT. In the latter case, the study may comprise a verification of P•FAT for selected crack configurations; contact person Vidar Osen, LINKfr, Trondheim.


The chosen methods and tools are applied to available fatigue test data, e.g., from the open literature and from the Joint Industry Project (JIP) ‘Fatigue of Girth Welds’; contact person Agnes Marie Horn, DNV, Høvik. The latter project has collected and documented fatigue data from 1084 full scale tests and 109 strip sample tests.

The thesis should include the signed problem text, and be written as a research report with summary both in English and Norwegian, conclusion, literature references, table of contents, etc. During preparation of the text, the candidate should make efforts to create a well arranged and well written report. To ease the evaluation of the thesis, it is important to cross-reference text, tables and figures. For evaluation of the work a thorough discussion of results is appreciated.

Three weeks after start of the thesis work, an A3 sheet illustrating the work is to be handed in. A template for this presentation is available on the IPM's web site under the menu "Undervisning". This sheet should be updated when the Master's thesis is submitted.

The thesis shall be submitted electronically via DAIM, NTNU's system for Digital Archiving and Submission of Master's thesis.

Contact persons are Agnes Marie Horn, DNV, Høvik, and Vidar Osen, LINKftr, Trondheim.


Torgeir Welo
Head of Division



NTNU
Norges teknisk-
naturvitenskapelige universitet

Institutt for produktutvikling
og materialer


Gunnar Härkegård
Professor/Supervisor

Appendix: References

References

1. S. Suresh, *Fatigue of materials*. Cambridge University Press, 1998. ISBN: 9780521578479
2. L. Molent and S.A. Barter, The lead fatigue crack concept for aircraft structural integrity. *Procedia Engineering* Vol. 2, 2010.
3. D. Radaj, C.M. Sonsino, W. Fricke, *Fatigue assessment of welded joints by local approaches*, 2nd edition. Taylor and Francis, 2006. ISBN: 0849384516, 9780849384516
4. G. Härkegård, J. Denk, K. Stärk, Growth of naturally initiated fatigue cracks in ferritic gas turbine rotor steels. *International Journal of Fatigue*, Vol. 27, 2005, pp. 715-726.
5. Q.G. Wang, P.E. Jones, Prediction of Fatigue Performance in Aluminum Shape Castings Containing Defects, *Metallurgical and Materials Trans B*, 38B, 615-621, 2007.
6. A. Wormsen, A. Fjeldstad, G. Härkegård, A post-processor for fatigue crack growth analysis based on a finite element stress field. *Computer Methods in Applied Mechanics and Engineering*, Vol. 197, Nos. 6-8, 2008, pp. 834-845.
7. A. Fjeldstad, A. Wormsen, G. Härkegård, Simulation of fatigue crack growth in components with random defects. *Engineering Fracture Mechanics*, Vol. 75, No. 5, 2008, pp. 1184-1203.
8. W.S. Johnson, The history, logic and uses of the equivalent initial flaw size approach to total fatigue life prediction. *Procedia Engineering* Vol. 2, 2010.
9. M. Shirani, G. Härkegård, Damage tolerant design of cast components based on defects detected by 3D X-ray computed tomography. To be published in *International Journal of Fatigue*, Special Issue 'Fatigue Design & Material Defects', 2012.
10. M. Shirani, G. Härkegård, Casting defects and fatigue behavior of ductile cast iron for wind turbine components: A comprehensive study. To be published in *Materialwissenschaft und Werkstofftechnik*, 2012.
11. T. Lassen, N. Recho, Proposal for a more accurate physically based S-N curve for welded steel joints, *International Journal of Fatigue* 31 (1) (2009) 70– 78.
12. *Fatigue Design of Steel and Composite Structures: Eurocode 3: Design of Steel Structures. Part 1-9 Fatigue. Eurocode 4: Design of Composite Steel and Concrete Structures. European Convention for Constructional Steelwork (ECCS)*, October 2011. ISBN: 978-3-433-02981-7.

Abstract

The main goal for this thesis has been to perform fatigue life predictions on large components. Different methods were to be chosen and reviewed critically. Experimental data for girth welded pipes was assessed by means of a version of BS7910 which were modeled from scratch. This version was verified with results from CrackWise, and used to predict the fatigue life for load cases matching the selected experimental data. The fatigue assessment tool P-FAT was used to predict the fatigue life for the same experimental data, and the results were compared. Except for some deviations recorded for embedded cracks, a generally good agreement was found between the two tools.

Both the modeled BS7910 and P-FAT predicted conservative but accurate fatigue lives for the experimental data that had significant defects. They predicted non conservative results for specimens that did not have significant defects, when the initial crack depth was set to 0.1 mm. When the initial crack depth was set to 0.5 mm the modeled version predicted fatigue lives in agreement with the experimental results.

Fatigue life predictions were also performed by assistance of $S-N$ curves provided by DNV-RP-C203. The results from these predictions were in agreement with the experimental data, except for four specimens. These four specimens had significant flaws, which reduced the fatigue life significantly.

A review of a two-phase fatigue assessment model was made. This model uses a strained based approach to assess the fatigue crack initiation phase, and the fracture mechanic approach suggested in the BS7910 to assess fatigue crack growth. This method have shown promising results for fatigue assessment of fillet welds in the literature, but the model needs further investigation and calibration to be used to predict fatigue life of girth welded structures. A specific area to investigate is the proposed transition depth of 0.1 mm. This depth is dubious based on the results

Abstrakt

Formålet med denne hovedoppgaven har vært å utføre utmattingsanalyser på store komponenter. Ulike metoder skulle velges og vurderes kritisk. Eksperimentelle data for 14 rundsømsveisede rør ble vurdert ved hjelp av en versjon av BS7910 som ble modellert opp fra bunnen av. Denne versjonen ble verifisert med resultater fra CrackWise, og ble deretter anvendt på lasttilfeller som simulerte de eksperimentelle dataene. Utmattingsprogrammet P-FAT ble brukt til å estimere utmattingslevetiden for de samme lasttilfellene, og resultatene ble sammenlignet med resultatene fra den oppmodellerte BS7910. Bortsett fra noen få avvik for indre sprekker, samsvarte resultatene.

Både den oppmodellert BS7910 og P-FAT predikerte konservative, men tilstrekkelig nøyaktige, levetider for de gitte lasttilfellene. Begge predikerte ikke-konservative resultater da den initielle sprekkybden ble satt til 0,1 mm, for prøvene som ikke hadde defekter av betydelig størrelse. Når den initielle sprekkybden ble satt til 0,5 mm, predikerte den modellerte versjonen av BS7910 utmattingslevetider i samsvar med de eksperimentelle resultatene.

Utmattingslevetiden ble også predikert ved hjelp av $S-N$ kurver fra DNV-RP-C203. Resultatene fra disse predikasjonene var i samsvar med de eksperimentelle resultatene, bortsett fra for fire prøver. Disse fire prøvene hadde defekter av betydelig størrelse, som reduserte utmattingslevetiden betraktelig.

En to-fase modell for vurdering av utmattingslevetid ble gjennomført. Denne modellen benytter en tøyingsbasert tilnærming for å anslå initieringstiden til en utmattingssprekk, og en bruddmekanisk modell i henhold til BS7910 for å vurdere den påfølgende sprekkeveksten. Denne metoden har vist lovende resultater for vurdering av utmatting i kilesveiser, men modellen trenger videre undersøkelse og kalibrering, for å kunne brukes til å forutsi utmattingslevetiden for rundsømsveiste konstruksjoner. Et spesifikt område som krever videre undersøkelse er dybden der sprekken går fra initierende til propagerende sprekke.

Contents

Prephase and acknowledgments	i
Abstract	v
Abstrakt	vi
Nomenclature	ix
1 Introduction	1
2 Theory	2
2.1 Welding flaws	5
2.2 Residual stresses in welds	5
2.3 Estimating fatigue life	6
3 Material database	9
3.1 Chosen data points	10
4 Fatigue life assessment of the selected specimens	15
4.0.1 Introduction	15
4.1 BS7910	15
4.1.1 Fatigue assessment of girth welds by means of theBS7910	16
4.1.2 Validation	18
4.1.3 Predicting fatigue life for the selected specimens	21
4.2 DNV-RP-C203	26
4.2.1 Introduction	26
4.2.2 Fatigue life predictions of the selected specimens based on DNV- RP-C203	27
4.3 P-FAT	28
4.3.1 Introduction	28
4.3.2 Predicting fatigue life of the selected specimens with	32
4.4 Two-Phase model	35
4.5 Discussion on the fatigue life prediction models	37
5 Conclusion	39
5.1 Future work	39
Referanser	40
A Comparison of geometry factor F for the modelled BS7910 and Crack- Wise	i
A.1 Surface cracks	i
A.2 Surface cracks	ii

B Comparison of geometry factor F and a/c for the modelled BS7910 and P-FAT

v

Nomenclature

JIP - joint industry project

PSB - percipient slip band

K - stress concentration factor

σ_m - mean stress

σ_a - stress amplitude

σ_{max} - maximum stress

σ_{min} - minimum stress

R - R ratio

IS/OS- inner surface/outer surface

AW – as welded

TIG – TIG dressed

a - crack depth

c - crack length

$\Delta\sigma$ stress range

ΔK – stress intensity range

F - geometry factor

W -plate length

L - distance from centre of crack to free surface

p - distance from crack depth tip to free surface

w - weight function

Chapter 1

Introduction

Components of different types subjected to alternating loads can experience crack initiation, growth and in the end final fracture. The crack initiation can even start at stresses well below the strength of the material. This process of initiation and growth of cracks due to cyclic loads is called fatigue. Designing machines and structures to avoid fatigue has been a subject for engineers for over 100 years. In the middle of the 19th century August Wöhler investigated fatigue failures in railroad axel. He found that the cyclic strength of steel axels were lower than the static strength. Welds are in many cases more sensitive to cyclic loading than the base material. In addition to a change in the mechanical properties in the weld compared to the base material, the weld can contain locally higher stresses due to changes in the geometry and welding defects. The fatigue life consists of two main phases, the initiation of a fatigue crack, and propagation of the crack. Many models have been developed to predict fatigue life. These models can roughly be divided into three main approaches, the stress based approach, the strain based approach and the fracture mechanic approach. The two first approaches are typically used to do full complete fatigue life estimations. The fracture mechanic approach on the other hand focus on crack propagation from an already initiated crack.

In this thesis a fatigue life predictions of large welded pipes have been performed. The predictions made have been compared with the results from a test data base. A short introduction to theory is given in chapter 2. A review of a material data base containing test results from fatigue tests of welded pipes are reviewed in chapter 3. In sections 4.4.1 and 4.4.3 fatigue life predictions based on the fracture mechanic approach have been conducted. In the first section recomondations from the BS7910 have been used to model fatigue crack growth in pipes and validated. In the latter section the fatigue assessment tool P-FAT have been examined. A stress based approach in form of $S-N$ design curves are examined in section 4.4.2. All these methods have been used to predict the fatigue life of a selection of specimens from the data base. In section 4.4.4 a two-phase model is reviewed. All models are compared and reviewed and recommendations for future work are proposed.

Chapter 2

Theory

In this chapter a short introduction to fatigue of materials is presented. The main focus is on fatigue in welded components in this chapter, this because the experimental data which are going to be assessed in this thesis represent girth welded pipes . This because fatigue assessment of welded structures, is the focus of this thesis. The theory in this chapter is mainly based on [1], [2], [3], [4] and [5], if nothing else is specified.

Fatigue damage accumulation is acquired by alternating loading on a component that leads to a locally alternating stress. This damage accumulation can happen even at stresses well below yield strength of the material. This damage accumulation due to the alternating stresses is fatigue. The fatigue process can mainly be divided into the following steps:

- permanent microstructural damage
- the creation of microscopic crack
- growth and coalesce of microscopic cracks or flaws into dominant crack
- stable crack propagation
- failure in form of structural instability or final fracture

These five steps can be further divided into three main phases of the initiation of a fatigue crack, crack growth and failure respectively. Where the three first sections can be categorized as the crack initiation phase, stable crack propagation is crack growth phase and the last phase is failure. All real life components will not progress as far as failure, a reason for this is that fatigue cracks found during inspections might lead to mending of or replacing of the component. Thus the two most important phases might be considered as the initiation and the crack growth phase. Though crack initiation and crack growth are two distinct phases the transition between the two are not exact. Scientists will perhaps consider flaws or cracks with the size of a micrometer as the transition between the two phases, while engineers will tend use a crack depth in the lower range of what it is possible to detect with non destructive inspection (NDI) equipment. This is usually in range of 0.1 mm and 1 mm. Fatigue life is defined as the sum cycle it takes to initiate a fatigue crack plus the number of cycles it takes to propagate a crack from an initiated crack to

failure. The number of cycles spent in the initiation phase can be as high 80% of the fatigue life for close to defect free components with smooth surfaces. How much of the fatigue life which is spent in the initiation phase depends on several factors, where stress gradients due to notches and radiuses, material property, geometry, the size and number of defects are the most relevant.

At a microstructural level a fatigue crack starts with dislocations. Dislocations will when applied stress move in the most favourable slip plane, with regards to loading direction and lattice structure. If thousands of dislocations move together they form a slip line. A cluster of slip lines is called slip band [6]. A slip band can with assistance of a microscope be visible at the free surface. During cyclic loading some of these slip bands get more pronounced and visible even if the free surface is electro polished. These bands are called persistent slip bands (PSB). Protrusions and intrusions forms within these PSBs. A protrusion is a slip “peak” while an intrusion is a slip “valley”. Figure 2.1a) illustrates a step case formation of slip produced by monotonic loading, while figure 2.1b) illustrates protrusions and intrusions within a PSBs formed by cyclic loading. Protrusions and intrusions produce stress gradients, this makes the adjacent area more pronounced to crack initiation, an example of such initiation is shown in figure 2.2.

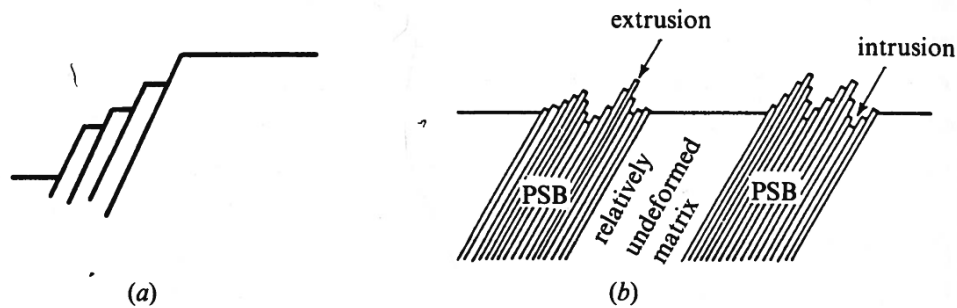


Figure 2.1: Figure a) [1] displays a step alike slip band formation produced by monotonic loading, while b) [1] displays PSB with protrusions and intrusions formed by cyclic loading.

There exists models that can be used to model crack initiation based on dislocation theory. Two examples are the models the one proposed by Rice [7] and the one proposed Hansson [8]. Though these models provide explanations to how a crack initiates and the early growth of a crack, they have limitations from an engineering point of view. First of all they predict the crack initiation at an already existing crack tip, not a free surface. The second limitation is that they are not really applicable to full size components for engineering purposes. They might not be applicable because both models use a known set of slip planes. For estimating fatigue life in full size components by either of these models the size and orientation of grains in locations vulnerable to fatigue crack initiation would be required. This is not always feasible. Since engineers tend to prefer relative simple and conservative models, these might also be too complicated or comprehensive to be preferred by the industry.

Another drawback with dislocation models is that they often require smooth surfaces to be applicable. Surface conditions play an important role determining the fatigue life. Unevenness at surface produces local stress gradients that might lead to crack initiation and further crack growth. This is true not only for protrusions and intrusions at a micro

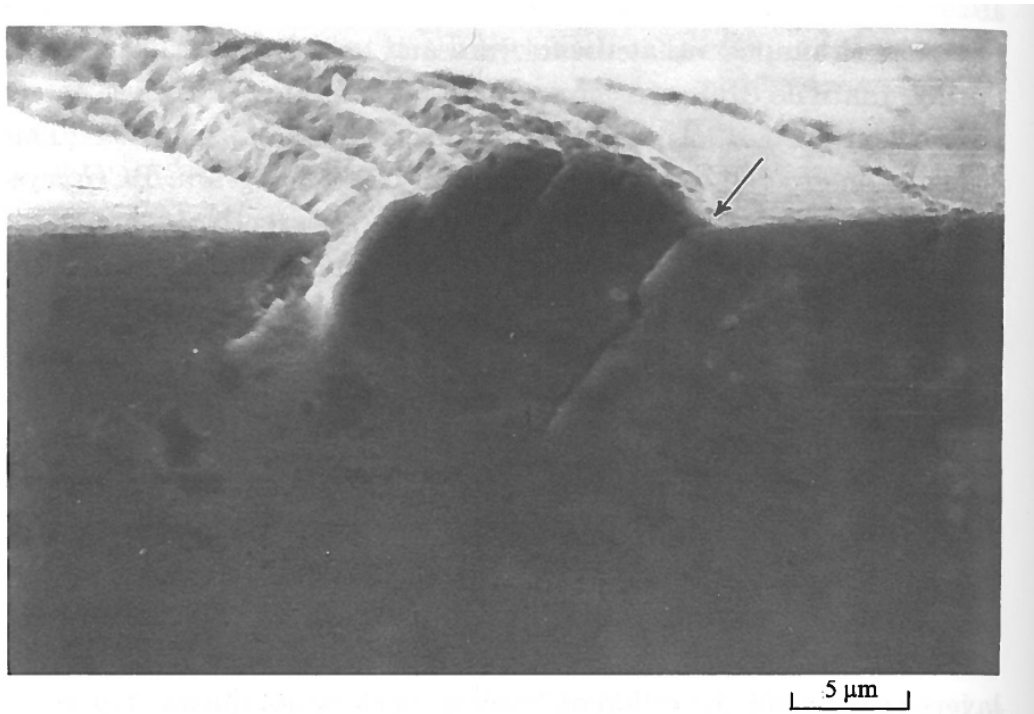


Figure 2.2: The picture [1] shows a crack (arrow) at the interface between the PSB and the surrounding material.

scale, but also at the macro scale, such as rivet holes, notches or other radii. This is especially important for estimating fatigue life for welded components, since welds that have not been through post weld treatments as grinding might suffer from rough surfaces. Not only surface roughness at the weld surface or in the transition between base metal and the weld but also weld spatter on the base metal. A schematic illustration of a butt weld is shown in figure 2.3.

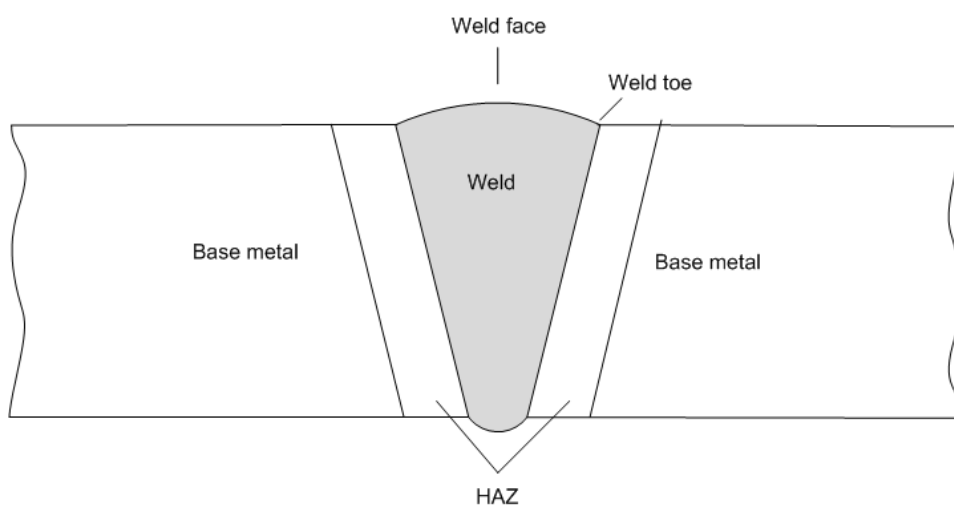


Figure 2.3: An schematic illustration of a butt weld. The HAZ is the heat affected zone.

2.1 Welding flaws

Welding defects and flaws have a considerable impact on the fatigue life. The reason for this is that welds have often much higher concentration of defects than forged materials. Welds can include a range of different type of defects or flaws, such as pores, undercut, inclusion, lack of fusion (LoF) and cold cracking to mention a few. Welding defects and flaws affects the fatigue properties in several ways. Type, size and the location of welding defects have a great influence on the fatigue life of components. The type of welding defects in a weld are result of different welding parameters, such as welding method, base and weld material, and welding environment are some. All these parameters and more affects the weld quality. Some of defects are:

- **Lack of fusion (LoF) or incomplete fusion** is lack of bonding between the weld and the base material or between different weld beads.
- **overlap** is when the weld overlaps the base material.
- **undercut** is when there is an indent in the weld at the intersection between the weld and the base material
- **porosity** is due to pores created in the weld.
- **lack of penetration** is when the weld does not penetrate through the desired thickness of the material.
- **inclusions** are compounds due to oxides, flux or electrode coating trapped in the weld.

The welding defects described above are illustrated in figure 2.4. In this thesis defects of significant and detectable size, which can be idealised as crack are denoted as *flaws*. Welding defects can be widely scattered, and statistically evaluation is therefore often recommended. Today it is possible detect weld defects through non destructive examination (NDE). Through this type of examination types, sizes and locations of the defects can found to some extent. While surface cracks in some cases can be mended or removed, internal defects are more difficult to remove. All defects can work as stress raisers and cause a crack to initiate. A good weld quality is therefore important to ensure sufficiently long fatigue life for a component.

2.2 Residual stresses in welds

Residual compressive and tensile stresses in welds are introduced as the welds cools down. These stress components arrive both parallel and normal to the welding direction as displayed in figure 2.5. As can be seen from the same figure the tensile residual stresses occur in the center of the weld, while the compressive residual stresses occur away from the weld centre. It is the contraction of the weld material that leads to these stresses. If the a weld has not been subjected to post weld heat treatment, the maximum stress in a fatigue loading cycle will be close to the yield stress of the material, regardless of the value of mean stress value is applied. These tensile residual stresses will therefore reduce

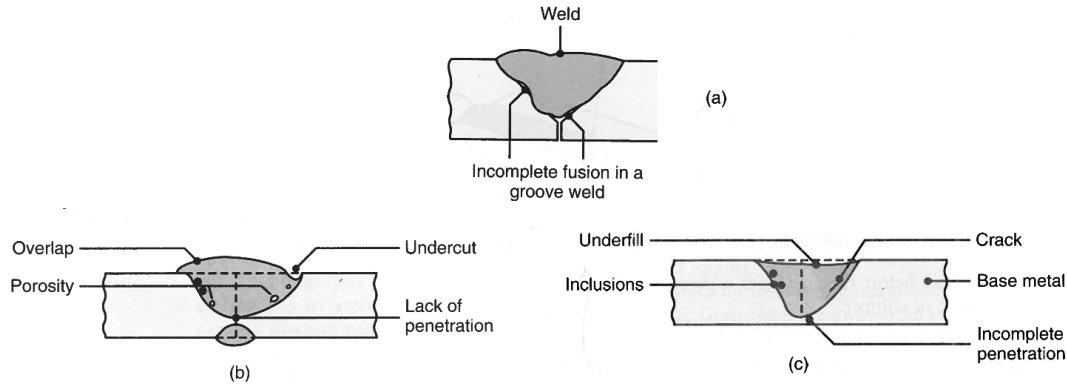


Figure 2.4: Figure a-c [9] displays different types of common welding defects.

the fatigue life of a welded component. In other words the weld is no longer sensitive to the applied stress ratio R . If post weld heat treatment has been performed on a weld, the weld will become sensitive to the applied stress ratio. Grinding also introduces residual stresses in the grinded are, both residual and compressive residual stresses. Though a flush ground grinded weld has lower stress gradient due to removal of the weld toe, it might introduce tensile residual stresses in locations vulnerable to fatigue cracking. Post grind heat treatment can reduce these residual stresses.

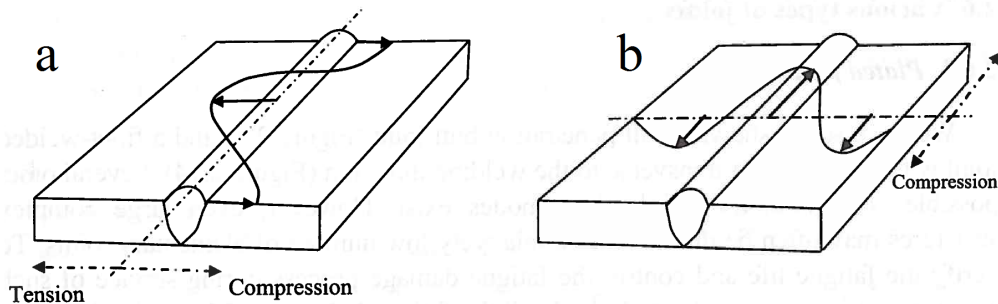


Figure 2.5: The typical distribution of residual stress normal to the weld is shown in a), while the typical distribution of residual stresses parallel to the weld is shown in b). [4]

2.3 Estimating fatigue life

A fatigue loading cycle has a given maximum stress σ_{max} and minimum stress σ_{min} value. If the stress levels have a constant minimum and maximum stress value it is called constant amplitude loading. The basic parameters for fatigue life calculation are the stress range the $\Delta\sigma$, the mean stress σ_m , the stress amplitude σ_a and R ratio and are given by:

$$\sigma_m = \frac{\sigma_{max} + \sigma_{min}}{2} \quad \sigma_a = \frac{\Delta\sigma}{2} = \frac{\sigma_{max} - \sigma_{min}}{2} \quad R = \frac{\sigma_{min}}{\sigma_{max}} \quad (2.1)$$

Together with material parameters these expressions form the foundation for most fatigue life calculations.

The use of $S-N$ curves to predict fatigue life is perhaps the most common way to predict fatigue life for components. To construct a $S-N$ curve several fatigue tests have to be performed at different stress ranges. The results are then usually plotted in a log-log diagram, with the stress range or amplitude at the y-axis and cycles to failure on the x-axis. Fatigue test specimens are usually both smooth and small compared to real size components. Because these specimens are small and smooth the results from such test cannot be directly applied to full size component. Recommended practices such as DNV-RP-C203 have built these considerations into their $S-N$ curves. $S-N$ curves are given for a R value. To perform fatigue life test with many different mean stress values, is neither practical nor economical. Different ways to handle mean stress have therefore been developed over the years. One way to handle mean stress effect is by using Walker equation:

$$\sigma_{a(R=-1)} = \sigma_{max} \left(\frac{1 - R}{2} \right)^\gamma, \quad (2.2)$$

where $\sigma_{a(R=-1)}$ is the stress amplitude for zero mean stress, R are the stress ratio, σ_{max} is the maximum stress and gamma is a material parameter. $S-N$ curves are a good tool for performing fatigue life assessments. But it has its limitations. It should be noted that $S-N$ curves provides no information regarding fatigue crack growth. To do fatigue crack growth analysis the introduction of fracture mechanics unit of stress intensity factor K have proven very useful. The K is a measure of the intensity the crack has on the surrounding material. A component can resist a fracture from a crack as long as the K is lower than the critical stress intensity for the material K_c . The stress intensity has three different modes, K_I , K_{II} , and K_{III} . The mode is dependent on load case, as illustrated in figure 2.6. The stress intensity factor for mode I loading can be calculated by:

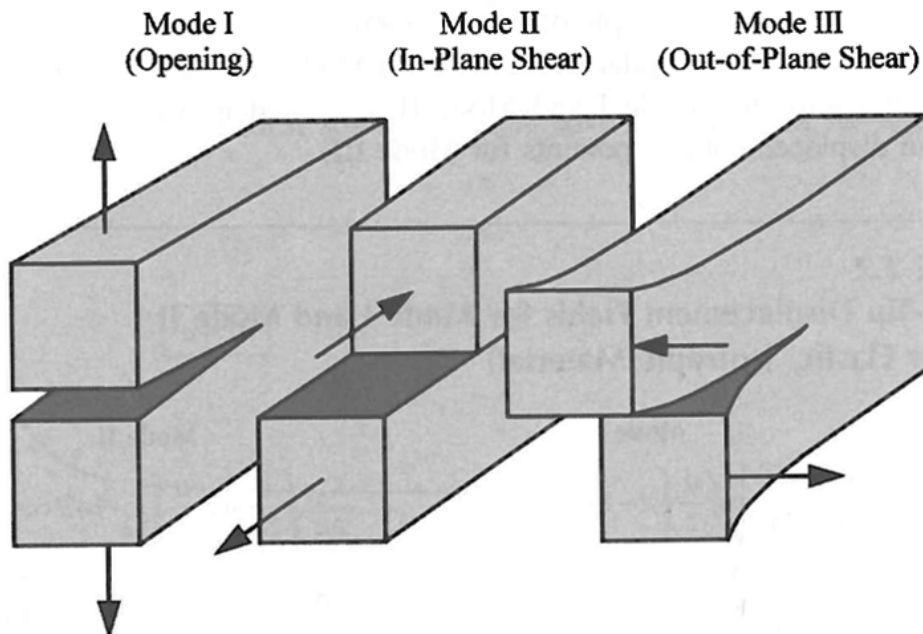


Figure 2.6: The figure [2] illustrates the three different stress intensity modes.

$$K_I = F\sigma\sqrt{\pi a} \quad (2.3)$$

where a is the crack depth for surface cracks or half the crack depth for internal cracks, as illustrated in figure 2.7. σ is the nominal stress. F is the geometry factor which depends on geometry and type of loading. In this thesis the expression crack depth will denote the length of the crack normal to the closest surface, illustrated as a in figure 2.7. The crack length c will be used to the length of the crack parallel to the closest surface, as illustrated in the same figure. If the nominal stress σ in equation 2.3 is substituted with

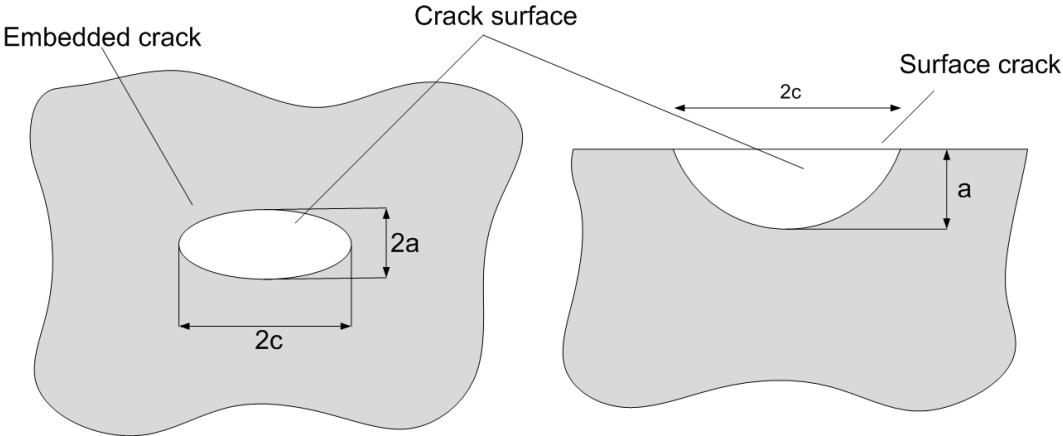


Figure 2.7: Illustration of two cross sections. The left cross section contains an embedded crack, while the right includes a surface crack.

the stress range $\Delta\sigma$ the stress intensity range for general mode is found as:

$$\Delta K = F\Delta\sigma\sqrt{\pi a} \tag{2.4}$$

Chapter 3

Material database

In this study fatigue data from a comprehensive database built up during an ongoing Joint Industry Project (JIP) has been evaluated and used. A JIP is project that is founded and funded by several different companies with one common interests and needs. The database contains data from girth welds. A girth weld is a butt weld joining to circular objects of the same diameter together, such as two pipes as illustrated in figure 3.1. The database consists of both data from recent as well as older tests. The tests have been performed at different locations with different materials as well as geometry. Full scale

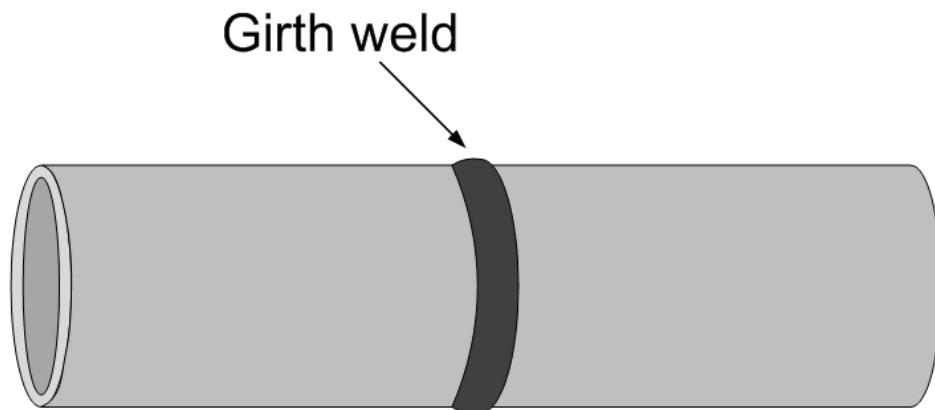


Figure 3.1: Schematic illustration of an girth weld.

test data from 1099 welds and 110 strip samples are included in the database. All full scale test specimens were joined pipes of different dimension. Physical information on the specimens such as nominal diameters, wall thickness, weld quality or weld curve in addition to material name is available. Though material names are given such as X60 and A707-L5, no specific information about material properties was included, except that they fulfill a minimum requirement. From a scientists point of view this is unfortunate, since such information would have made it easier to compare different fatigue life models with the results found in the data base. This is because different models require different material parameters, and therefore lack of material parameters will restrict the numbers

of models it is possible to apply to the data. Engineers on the other hand, they want to use applicable models that require as few parameters as possible, which can be categorized in standards.

A few of the specimens contained forged instead of welded joints. Some specimens were reeled. Most data points from the full scale tests contained information on whether the joints were grinded ground flushed to a smooth surface either on the inside, outside, both or neither. Nominal stress, mean stress values and stress ranges and fatigue life data were available for all specimens. Information regarding if the initial crack was located on the inside or the outside were also available for most of the specimens. Final crack size was recorded from some. There were pictures of most of the test specimens. Some showing the crack surface while others showed specimen configuration and dimensions.

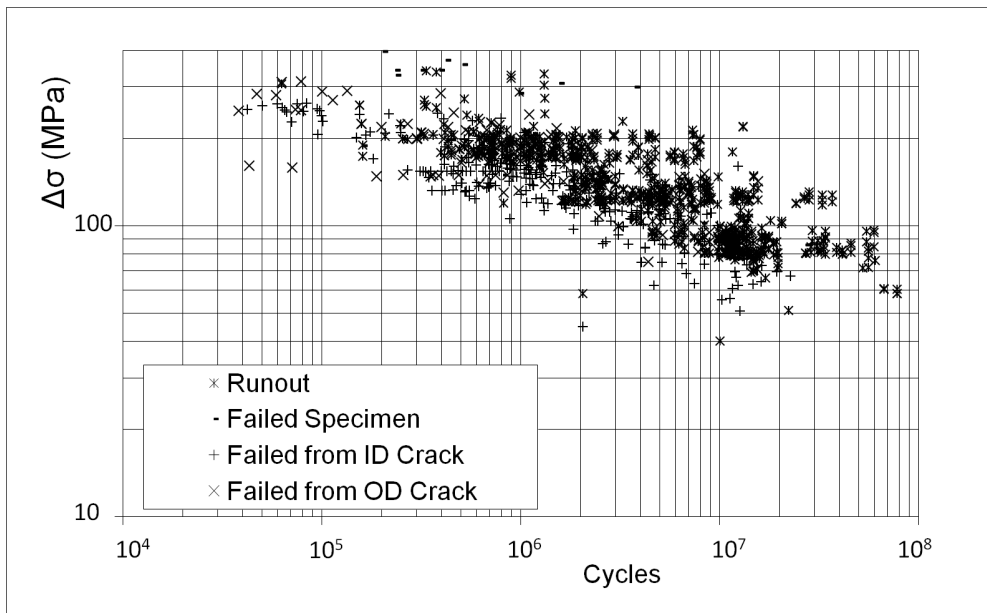


Figure 3.2: Plot showing all data points from the JIP database.

3.1 Chosen data points

As mentioned earlier the data set was quite comprehensive. As illustrated in figure 3.2 the dataset contained large amounts of data points. Many of these represent as described earlier different dimensions and materials. The number of specimens to use in this thesis was therefore limited to fourteen specimens. From now on these specimens will be referred to as *the selected specimens*. The tests of these fourteen specimens were conducted by DNV in the early 90s. The reason for choosing these data points were that there was additional information available for these specimens. Every failed specimen had been examined after failure. Metallographic pictures were available for some of the specimens. Crack growth had been recorded for some of the specimens. Information on initiation point of the fatigue crack was also available. If the crack initiated at a defect, the dimension of this and surrounding defects were documented by both text and pictures. This meant that a fracture mechanic crack growth model could be applied directly. Each test specimen

contained three girth welds.

All fourteen specimens had the same geometry and dimensions, which can be seen in figure 3.3. All fourteen specimens had outer diameter of 609.6 mm, a wall thickness of 20.6 mm, and all tests were run in air. Two of the test specimens 1 and 2 were tested

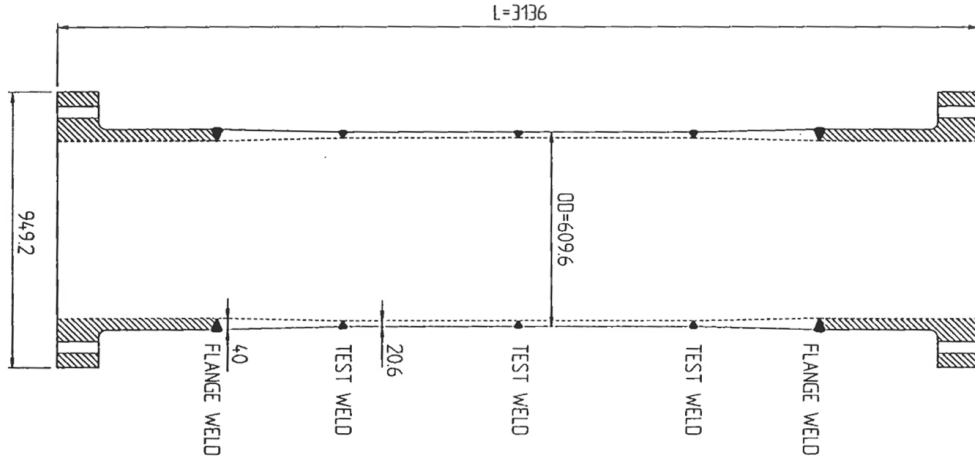


Figure 3.3: Schematic illustrations of the cross section of the test specimens. All dimensions are given in mm.

as welded, while test specimens 3 to 11 had ground flush welds both on the inside and outside of the pipe. Specimens 12 to 14 were TIG dressed both at inside and outside. Information on the specimens are given in table 3.1. Fatigue curves according to DNV-RP-C203 [10] are displayed in the same table. All specimens were loaded in air in tension, and all the failed specimens failed in area of the girth weld. The pipe material was X60-TMCP carbon steel. The X60 indicates the lowest yield strength allowed according to the material specification code. It must be emphasized that yield strength is not the only requirement for the X-60 series. The numbers indicate yield strength in ksi. This means that this X60-TMPC has at least yield strength of 413 MPa. TMCP indicates that the material has been undergoing a Thermo-Mechanically Controlled Processed. This means that during the manufacturing process of the pipes the temperature of the steel has been closely monitored and controlled. This is to ensure that the finished product has the desired mechanical properties. The selected specimens were further divided into two groups one containing specimens that had its main fatigue crack initiated at a flaw and therefore could be assessed with crack growth models. The information on these welds is available in table. 3.3. All the flaws were located circumferentially, normal to the loading direction. The information on the remaining welds that had initiation point at flaw free location are displayed in table 3.2. Some of the failed welds experienced multiple cracks. Compared to the main cracks these extra cracks were long and narrow, and never breached the both surfaces. Even though there existed multiple cracks in some of the specimens, it was chosen to not address these secondary cracks as the main focus of this thesis is not secondary cracks or defects. The fourteen specimens were subjected to different stress ranges and mean stresses as shown in the tables 3.3 and 3.2

Table 3.1: The table displays the information on the fourteen test specimens chosen from the JIP database. AW denotes as welded, IS and OS refer to grounded inner and outer surface respectively, while TIG refer to TIG dressing.

Specimen Number	Weld Number	Weld condition	Number of cycles applied	Weld curve	Outer Diameter (mm)	Wall Thickness (mm)	Material
1	1-1	AW	155000	D	609,6	20,9	X60-TMCP
	1-2						
	1-3						
2	2-1	AW	249000	D	609,6	20,9	X60-TMCP
	2-2						
	2-3						
3	3-1	AW	300000	D	609,6	20,9	X60-TMCP
	3-2						
	3-3						
4	4-1	IS,OS	158000	C1	609,6	20,9	X60-TMCP
	4-2						
	4-3						
5	5-1	IS,OS	2652000	C1	609,6	20,9	X60-TMCP
	5-2						
	5-3						
6	6-1	IS,OS	412000	C1	609,6	20,9	X60-TMCP
	6-2						
	6-3						
7	7-1	IS,OS	3089000	C1	609,6	20,9	X60-TMCP
	7-2						
	7-3						
8	8-1	IS,OS	4474000	C1	609,6	20,9	X60-TMCP
	8-2						
	8-3						
9	9-1	IS,OS	618000	C1	609,6	20,9	X60-TMCP
	9-2						
	9-3						
10	10-1	IS,OS	255000	C1	609,6	20,9	X60-TMCP
	10-2						
	10-3						
11	11-1	IS,OS	608000	C1	609,6	20,9	X60-TMCP
	11-2						
	11-3						
12	12-1	TIG	719000	C1	609,6	20,9	X60-TMCP
	12-2						
	12-3						
13	13-1	TIG	2011000	C1	609,6	20,9	X60-TMCP
	13-2						
	13-3						
14	14-1	TIG	Runout	C1	609,6	20,9	X60-TMCP
	14-2						
	14-3						

Table 3.2: The table contains information for the selected specimens that had the initiation point of the main fatigue crack located at a flaw.

Weld Number	First surface penetration	Crack initiation comment	$\Delta\sigma$ (Mpa)	$\Delta\sigma$ (Mpa)	Number of cycles	Crack size at end of test $2c$	Crack size at end of test a (mm)
1-2	Inner surface	Weld toe irregularity 0,3 mm deep, 60-70 mm long	159	260	155000	760	20.9 (through)
4-2	Outer surface	LoF defect 3x20 mm close to outside surface	137	225	158000	420	20.9 (through)
5-2	Outer surface	LoF defect 2x8 mm	92	150	2652000	1100	20.9 (through)
6-1	Inner surface	4 LoF defects 0,5x5 mm, 0,5x7 mm, 0,5x17 mm, 1x22 mm close to inside surface	107	175	412000	300	20.9 (through)
7-1	Outer surface	LoF defect 2x15 mm close to outside surface	61	100	3089000	483	20.9 (through)
8-1	Inner surface	LoF defect 0,4x1 mm close to inside surface	95	155	4474000	700	20.9 (through)
10-2	Embedded	LoF defect 7x16 mm	122	200	255000	750	20.9 (through)
11-2	Outer surface	LoFs defects 1x7 and 1x4 mm close to outside surface	107	175	608000	625	20.9 (through)

Table 3.3: The table contains information for the selected specimens that had the initiation point of the main fatigue crack located at an arbitrary point.

Weld Number	First surface penetration	Crack initiation comment	$\Delta\sigma$ (Mpa)	$\Delta\sigma$ (Mpa)	Number of cycles	Crack size at end of test 2c	a (mm)
2-3	Inner surface	No particular defect	137	225	249000	59	20.9 (through)
3-3	Outer surface	No particular defect	122	200	300000	230	20.9 (through)
9-1	Inner surface	No particular defect	122	200	618000	540	20.9 (through)
12-1	Inner surface	Slag inclusion 7x10 mm close to outside surface	107	175	719000	370	20.9 (through)
		seemed to have influenced crack initiation or propagation					
13-2	Inner surface	No particulare defect	92	150	2011000	650	20.9 (through)

Chapter 4

Fatigue life assessment of the selected specimens

4.0.1 Introduction

In this chapter different fatigue life assessment methods will be reviewed and tested on the selected specimens. First a modelled version of BS7910 will be considered. Then the $S-N$ approach suggested by DNVs design code will be reviewed. The last method is the fatigue assessment to tool P-FAT, where the single defect module have been applied on the selected specimens. Another method suggested by Lassen and Recho have been reviewed, but not applied to the data from the selected specimens. In the end of the chapter a comparison of the different methods and tools is done.

4.1 BS7910

The British Standard 7910 (BS7910) contains procedures for how to assess acceptability of flaws in given types of structures and components. Although the BS7910 include procedures for a range of materials and joining configurations its main focus is welded connections in ferritic and austenitic steels. Flaws can by means of the BS7910 be assessed by the following failure mode or damage mechanism:

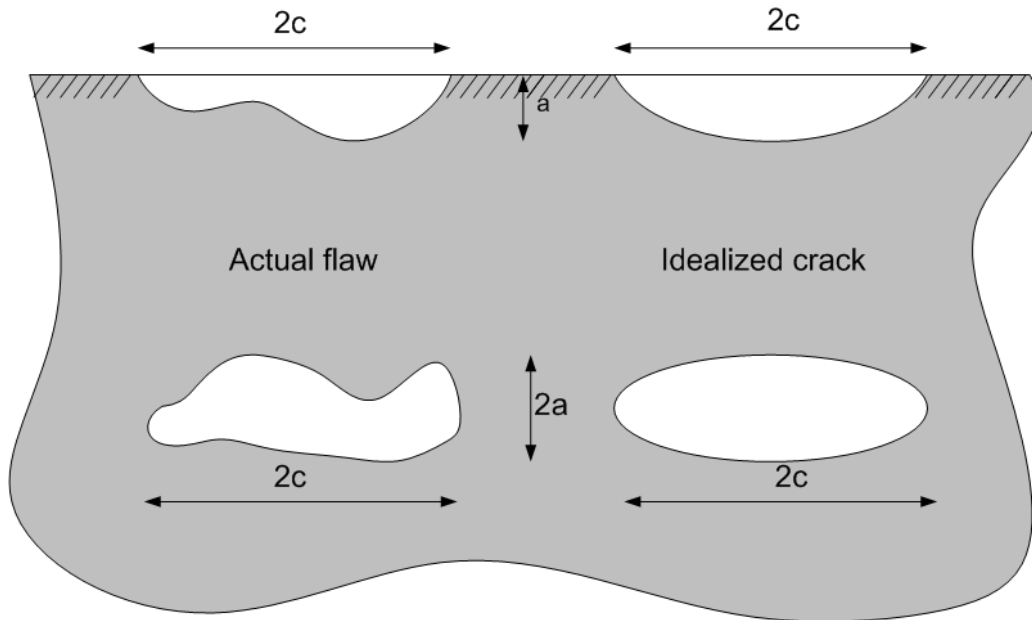
- failure by fracture or plastic collapse
- failure by leakage
- failure by instability
- damage by fatigue
- damage by creep
- damage by corrosion and erosion
- damage by environmental assisted cracking

In this thesis the procedures in BS7910 for flaw assessment by fatigue damage have been used to analyse the selected specimens. Data tools such as CrackWise and LinkPipe could have been used directly since they both have build in modules that are based on the procedures from the BS7910. In this thesis however an assessment tool for the given geometry of the selected specimens was modelled from scratch. This tool will now be denoted as *the modelled BS7910*, while the standard itself will be denoted just *BS7910*. The reason why the BS7910 was modelled from scratch was to give the author a better understanding of how the BS7910 assess flaws and recommend practice for fatigue life assessments. Thereby provide the opportunity to evaluate the results in more detail. The results from the modelled BS7910 were compared with the results from CrackWise 4.2, the results are displayed later in this section.

4.1.1 Fatigue assessment of girth welds by means of theBS7910

To assess flaws in welded structures the BS7910 include procedures for two different approaches, a simplified related to $S-N$ curves a general approach based on fracture mechanics. The latter will be used and evaluated in this section. By means of the fracture mechanic approach BS7910 idealizes a flaw as sharp crack. The shape is also idealized as show in figure 4.1. The BS7910 assumes that the idealized crack grows in accordance

Figure 4.1: The figure illustrates a surface and an embedded flaw to left and the appurtenant idealized cracks to the right



with the well known Paris law, which relate crack growth rate and stress intensity range. The Paris law is:

$$da/dN = C(\Delta K)^m, \quad (4.1)$$

where C and m are material parameters which are dependent on material, loading, and loading environment. da/dN is the crack growth rate, describing how fast the crack grows for a certain ΔK . ΔK is the stress intensity range and a function of the structures

geometry, stress range, loading mode and crack size and is calculated by the following equation:

$$\Delta K = F \Delta \sigma \sqrt{\pi a} \quad (4.2)$$

Here $F, \Delta \sigma$ and a are geometry factor, stress range and crack depth respectively. BS7910 predicts no crack growth if the ΔK falls below the stress intensity range threshold, ΔK_{th} :

$$da/dN \text{ is assumed zero for } \Delta K < \Delta K_{th} \quad (4.3)$$

The geometry factor F is a function of crack size and type of loading. Inserting 4.2 into 4.1 the fatigue life can be calculated by integrating over the increase in crack depth in the following equation:

$$\int_{a_i}^{a_f} \frac{da}{F^m (\pi a)^{m/2}} = C (\Delta \sigma)^m N \quad (4.4)$$

In equation 4.4 the N is the number of cycles required to propagate a crack from an initial crack depth a_i to final depth a_f . Because F is dependent on crack size as well as geometry the F changes as the crack grows. The fatigue life can therefore not be calculated based on the initial and final crack depth alone. The calculation needs to be split into smaller increments where F is recalculated at each increment. BS7910 provides a procedure for how to define these crack increments Δa . This procedure is used in CrackWise. To calculate fatigue crack growth for relative long fatigue lives this procedure is good as it can reduce the number of calculation needed and thereby reduce the calculation time. For relative short fatigue life however it has less influence on calculation time. Computers nowadays have the ability to do millions of calculations in a relative short period of time. Therefore it was chosen to calculate the fatigue life by solving the equation by means of a_f instead of N in the modelled BS7910. Defining an increment as $N = 1$ and recalculating F at each increment. This is done to let F influence the crack at each cycle. Only a small deviation between the two methods is noticed, this will be discussed later. BS7910 provides equations for determining the geometry factor F for various geometries and loading cases, but allows also for well documented published solutions such as those by Murakami [11]. For the girth welds three different flaw or crack configurations needed to be assessed. These were embedded cracks in curved shells, surface cracks in curved shells and through thickness cracks in curved shells. For embedded cracks in BS7910 recommends in M 3.4 a flat plate solution. For membrane uniaxial loading in shells or cylinders without any stress raisers such as misalignment or weld toe angle the stress intensity range is given as:

$$\Delta K_{A,C} = F(a, c, B, p, W) \Delta \sigma \sqrt{\pi a}, \quad (4.5)$$

where A and C denotes the positions at the tips of the crack depths and tip at the crack lengths. a, c, p, B and W are units in mm as illustrated in figure 4.2b) For pipes the W is the perimeter of the pipe. For surface cracks the BS7910 propose two different solutions, which are dependent on if the crack is located on the inside or outside of a cylinder. This solution however is not valid for B/r_i ratio of the pipes in question, where B is the wall thickness and r_i is the inner radius of the pipe, as illustrated in figure 4.2 a). A solution proposed in M 4.2 in the BS7910, which is valid for curved shell was therefore used instead. This solution does not differentiate between surface cracks located on the inside or outside of the pipe. This is also the same solution that CrackWise uses. It

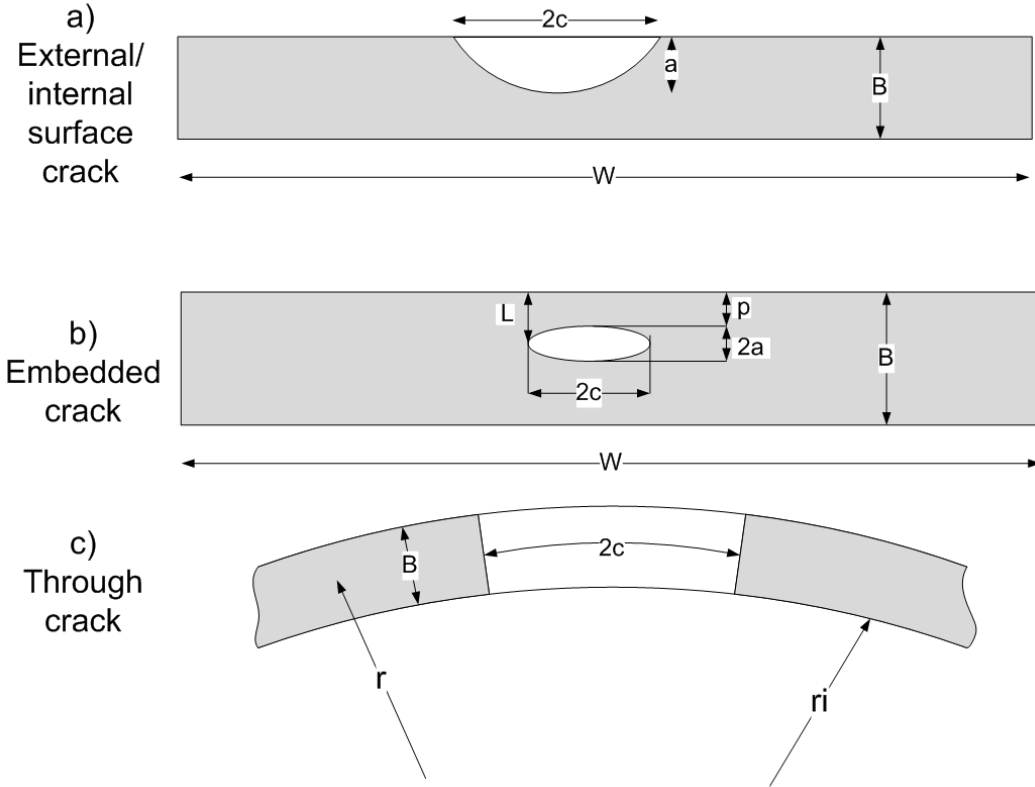


Figure 4.2: Figure illustrating the idealized situations in of a) surface b) embedded and c) through crack, used in the modelled BS7910.

calculates the ΔK as:

$$\Delta K = F(a, c, B, W) \Delta\sigma\sqrt{\pi a}, \quad (4.6)$$

where A and C denotes the positions at the tips of the crack depths and tip at the crack lengths. a , c , B and W are units in mm as illustrated in figure 4.2 For cracks that penetrate the full thickness of the pipe a simplification that is not proposed in the BS7910 was used in the modelling. This was done due to problems obtaining results in agreement of the results from CrackWise. The geometry F factor used in the modelled BS7910, contained only a correction for the area reduction due to the crack surface. This factor is taken from M.2 in the BS7910. The Δ then becomes:

$$\Delta K = F(c, r) \Delta\sigma\sqrt{\pi c}, \quad (4.7)$$

where c and r are units in mm as illustrated in figure 4.2. The BS7910 allows for re-categorization of a crack as soon as grows through a free surface. From embedded crack to a surface crack, making the new surface crack depth equal to two crack depths for the embedded crack.

4.1.2 Validation

The results from the modelled version of BS7910 were compared with results from CrackWise 4.2. Three different a/c relationship was compared for the cases of embedded crack

and for surface crack. A configuration of a through crack was also tested. The dimension of the geometry simulated the geometry for selected specimens. The reason for this was that it this geometry was the only geometry that was going to be analysed in this thesis. An illustration of the geometry is given in figure 3.3 but with one weld instead of three. The different test configurations are listed in table 4.1. a_i/c_i is the initial a/c relationship. A comparison between the development of a/c of the result from CrackWise and

Table 4.1: Table contains the parameters which was used to validate the modelled BS7910. The L is as illustrated in figure 4.2

	Embedded crack	Surface crack	Through crack
	a (mm) L (mm)	a (mm)	c (mm)
$a_i/c_i = 1$	1 5	1	-
$a_i/c_i = 0.5$	1 5	1	-
$a_i/c_i = 2$	2 4	2	-
$a_i \geq B$	- -	-	5

the modelled BS7910 for the surface cracks and the embedded cracks are given in figure 4.3 a) and b) respectively. As can be seen from the figures the a/c relationship behave in the same manner for the modelled BS7910 and CrackWise for both the surface cracks and the embedded cracks. This means that the two methods predict the crack will have the same crack size and shape as the crack grows.

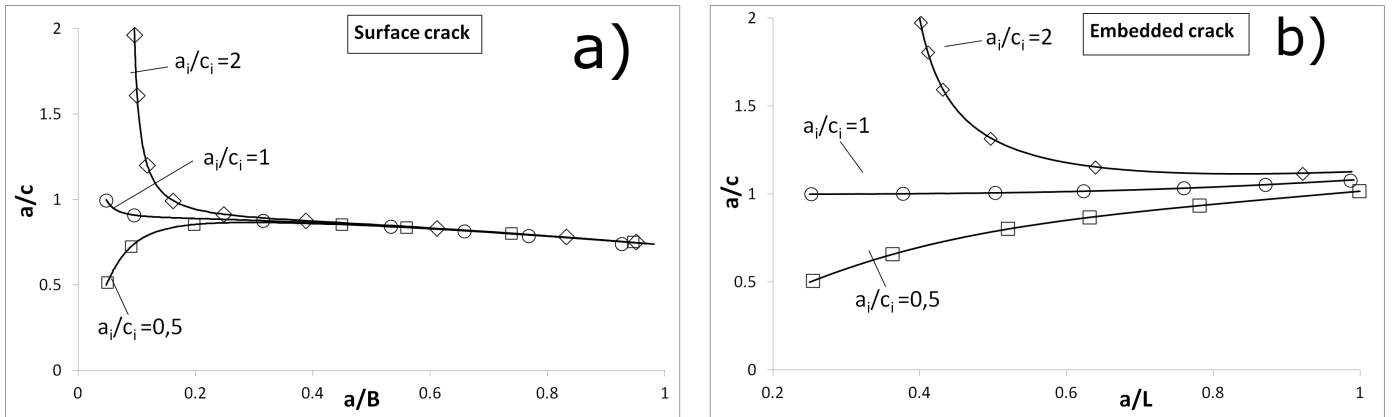


Figure 4.3: Figure a) displays the development of the a/c relationship for the three different initial a_i/c_i configurations for a growing surface cracks, while b) displays the same relationship for embedded cracks. The lines represent the results from the modelled BS7910, while the indicators are the results from CrackWise. B is the plate thickness while L is the distance from centre of the crack to the closest free surface

A comparison of the geometry factors F was also done. The F is found by solving equation 4.2 with regards to F :

$$F = \frac{\Delta K}{\Delta \sigma_{applied} \sqrt{\pi a}}, \quad (4.8)$$

where $\Delta \sigma_{applied}$ is the applied stress range. The comparison of the geometry factor for $a_i/c_i = 0.5$ for the embedded crack and the surface crack are found in figure 4.4 and 4.5 respectively. As can be seen in the figures the geometry factors are almost identical at

the early crack growth. After a while the geometry factor for CrackWise starts to deviate slightly from the calculated by the modelled BS7910. This behaviour is present for the six calculations for both surface and embedded cracks. The deviation for embedded cracks are less pronounced compared to the deviation for the surface cracks. The maximum deviation recorded was still under 6%. The deviation could be a result of the fact that CrackWise calculates the crack growth for an increment in a , while the modelled BS7910 has the increment set to one cycle. The deviation is also most pronounced when the crack grows close to a free surface. The number of cycles needed to propagate the crack a given distance Δa is less near the free surface than for the same distance Δa at the early crack growth. Hence the effect the deviation in geometry factor has on the calculated fatigue life should be small. It is important to emphasise that these numbers represent the geometry from figure 3.3, and is not the general behaviour of the geometry factor for different geometries. The figures for the rest of the comparisons of the geometry factor are found in appendix A. For through cracks the recorded deviation was higher. A deviation

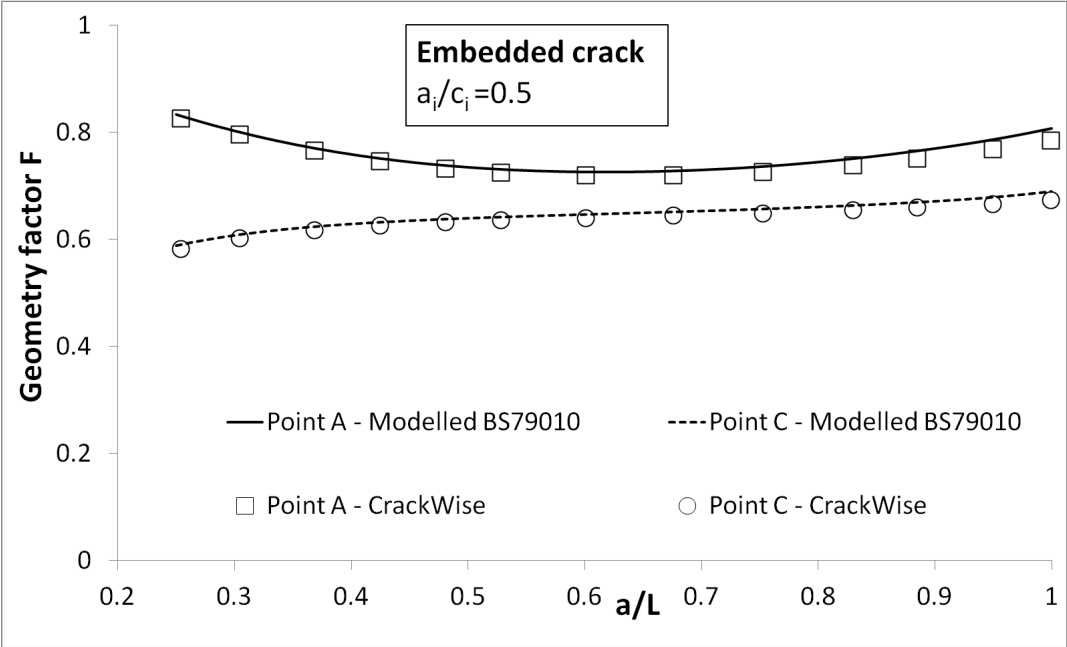


Figure 4.4: Geometry factor as the crack grows for calculations done by the modelled BS7910 and CrackWise for an embedded crack with initial a/c ratio of 0.5

of up to 60% was recorded for cracks for $2c \leq W = 0.5$, as shown in figure 4.6. As the figure illustrates the geometry factor for the two methods are comparable for low $2c/W$, but starts to deviate immediately as the crack begins to grow. Even though the deviations becomes as high as almost 60% , it was still chosen to be within acceptable limit for the purpose of this thesis. One of the reasons was that the number of cycles spent on propagating the through crack to its final length was few compared to the number of cycles spent in propagating the surface or/and embedded crack. A second reason was that for the deviation was smallest for relative short through cracks which would be where the most of the through crack fatigue life be spent.

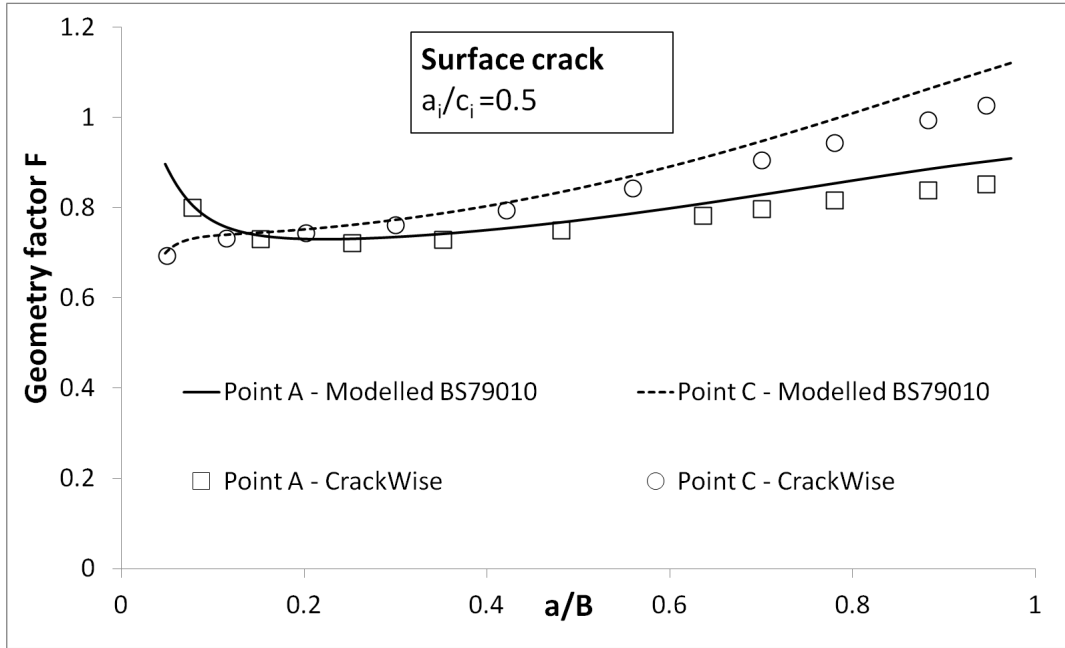


Figure 4.5: Geometry factor as the crack grows for calculations done by the modelled BS7910 and CrackWise for a surface crack with initial a_i/c_i ratio of 0.5.

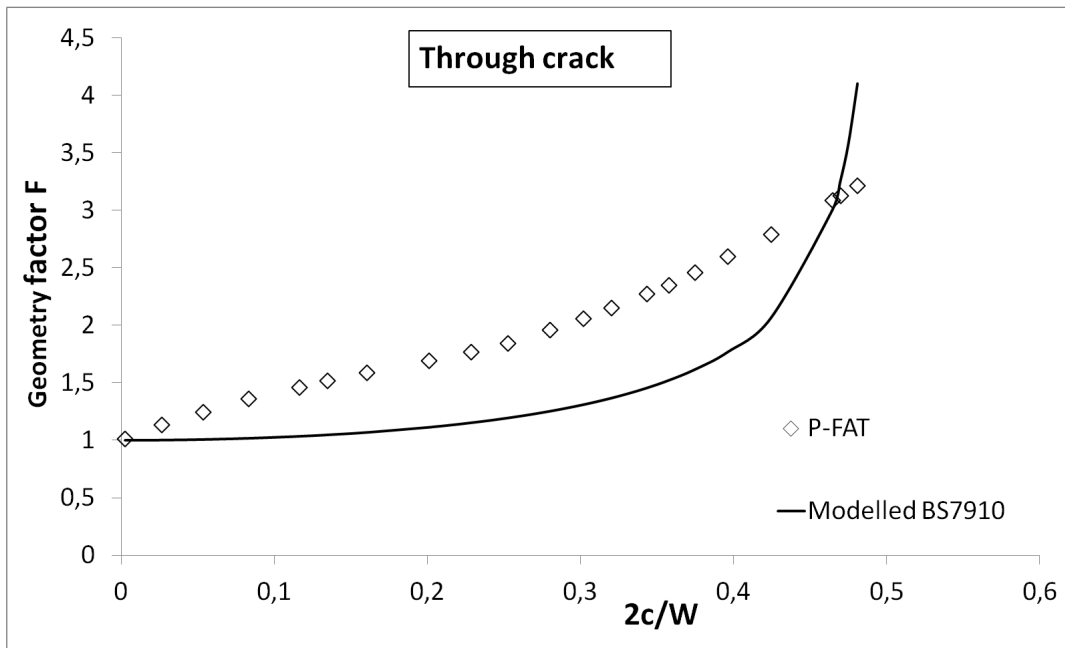


Figure 4.6: Geometry factor as the crack grows for calculations done by the modelled BS7910 and CrackWise for a through crack with initial length of $c = 5\text{mm}$

4.1.3 Predicting fatigue life for the selected specimens

The material parameters used in the modelled BS7910 to predict fatigue life was taken from the BS7910 standard. Two sets of parameters were used. The first and conservative set was the one representing the mean plus two standard deviations crack growth curve for steels in air for $R \geq 0.5$. Though all the selected specimens were loaded at $R = 0.1$,

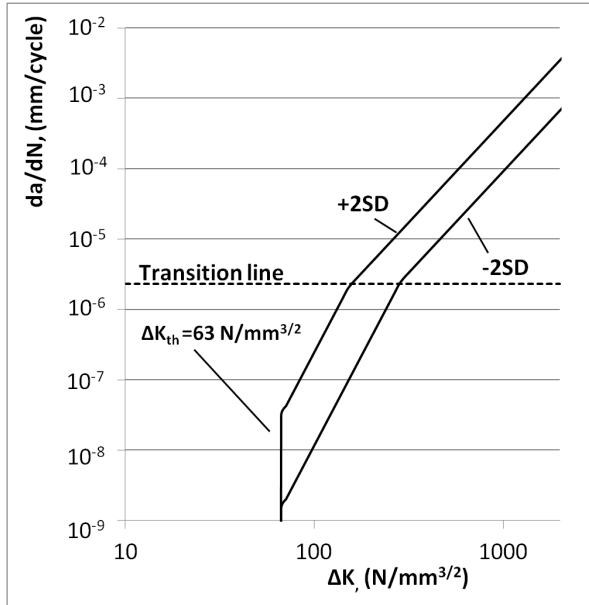


Figure 4.7: Crack growth curves for steels in air.

	Mean +2SD	Mean -2SD
m_1	5.10	5.10
C_1	2.10×10^{-17}	1.00×10^{-18}
m_2	2,88	2,88
C_2	1.29×10^{-12}	2.50×10^{-13}
T.P. (ΔK)	$144 \text{ N/mm}^{3/2}$	$270 \text{ N/mm}^{3/2}$

Table 4.2: Material parameters used in the modelled version of BS7910. T.P is a abbreviation for transition point, and marks the ΔK value where the transition between stage 1 and stage 2 behaviour is located.

BS7910 recommends use of parameters for $R \geq 0.5$ for welded structures. The reason for this is that as mentioned in the theory section, a weld that has not been subjected post weld heat treatment contains residual stresses that affect the mean stress value in the weld. The crack growth rate curve recommended by the BS7910 is a biaxial line, containing two stages. As mentioned earlier the crack will not grow as long as $\Delta K \leq \Delta K_{th}$. For ΔK over the threshold value ΔK_{th} the crack growth will increase relative rapidly before reaching a transition point at a given crack growth rate. From this point on the crack will grow rate will increase less rapidly as the ΔK increases. The first set of parameters is the mean +2 standard deviation (SD) crack growth curve. Because fatigue data tend to scatter a form of distribution is often used. The second set of material parameters represents the mean -2SD curve. This curve is not given explicitly in the BS7910 standard. The crack growth curve was estimated by using the data for the mean and the mean +2SD data. Both curves are displayed in figure 4.7.

The modelled BS7910 was used to predict the fatigue life for the selected data specimens. More information about the data points and the geometry can be found in section 3. The data points have been divided into two different categories, the first representing test data for specimens that had the main fatigue crack located at a flaw, and the second for specimens that had the main crack initiated at an arbitrary surface point on the weld. The reason for this is that the BS7910 contains procedures for assessing acceptability of flaws. Hence, it is not intended for assessing structures without significant flaws. An analysis of flaw free components are still performed to give shed some light upon the challenge with selecting a transition depth between initiation and propagation of fatigue crack. The results will be compared with a transition crack length proposed by Lassen and Recho [4] later.

Fatigue life prediction of specimens with flaws

First the results from the prediction of fatigue life of the specimens containing flaws will be reviewed. Descriptions of these specimens are given in 3.3. The results are displayed in figure 4.9. Both the predictions based on parameters from the mean -2SD crack growth curve and mean -2SD crack growth curve are included in the figure. As can be seen from the figure most predictions follow the same trend, being on the conservative side of the predicted results. The points representing the mean -2SD parameters are close to the test results. This indicates that these parameters are the one best suited to predict the fatigue life for the pipes based on the simplifications assumed. Another reason could be that the flaw shape has been idealized as shown in figure 4.1.

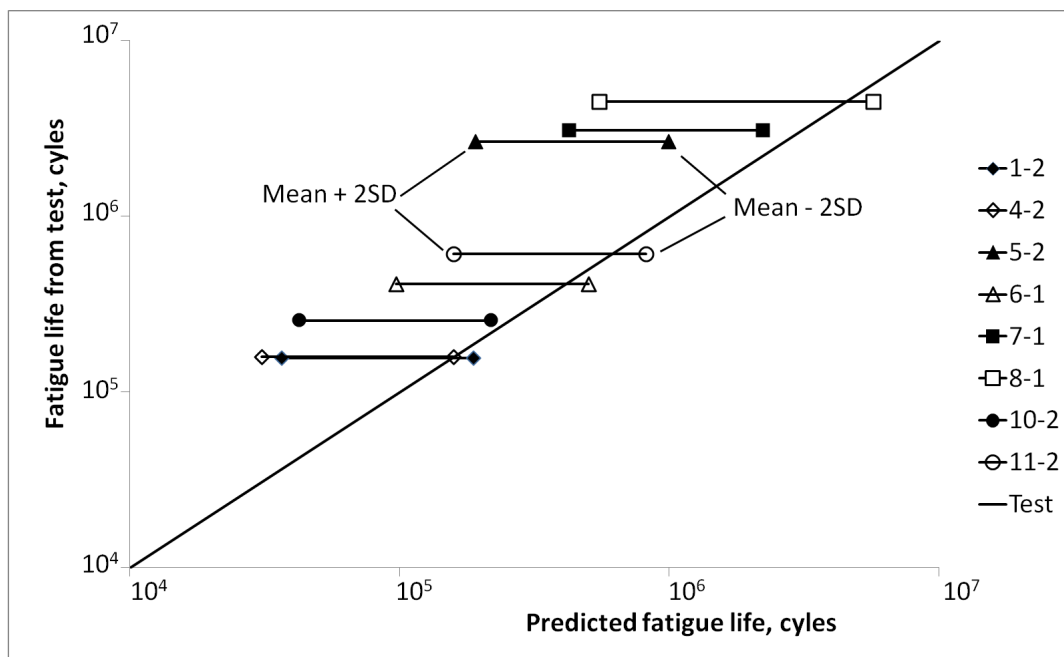


Figure 4.8: The figure illustrates the predicted fatigue life x-axis, versus the fatigue life from the tests for the flawed specimens. The left points indicated predictions done with mean plus 2SD parameters while the right points indicate predictions done with mean minus 2 SD parameters.

Fatigue life prediction of specimens without significant flaws

Even though the BS7910 does not cover structures without significant flaws, the modelled BS7910 was used to assess the test specimens without any significant flaws. An initial crack depth of 0.1 mm was assumed as proposed by Lassen and Recho [4] for fillet welds. The crack depth/ length ratio was set to $a_i/c_i = 1$. As for the flawed specimens predictions of the fatigue life with both mean minus 2 SD and mean plus 2 SD were performed. Figure 4.9 illustrates the predicted fatigue life versus the fatigue life from the tests. As for the results from the predictions of the flawed specimens these results follows a trend, but with a less conservative displacement on the plotted fatigue test results. Instead of being on the conservative side of the line representing the fatigue life, these results are located on

the non conservative side. Even the prediction based on the parameters for mean +2SD, which are the “worst case” parameters, gave non conservative predictions. This indicate that setting the transition depth to $a_i = 0.1$ might not be suitable for girth welds without any major stress concentration factor as can be found in fillet welds. Another argument is that the initial ΔK for specimen was lower than ΔK_{th} for weld 13-2, meaning it would not predict any crack growth at all. A prediction was still made as the figure shows, this was done with a slightly lower ΔK_{th} .

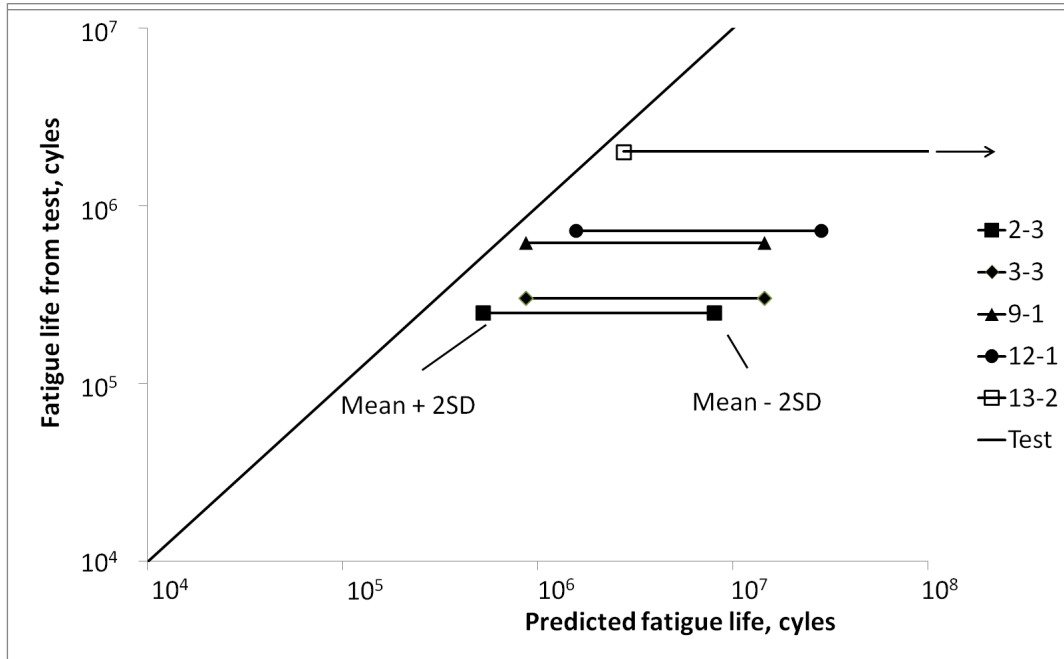


Figure 4.9: The figure illustrates the predicted fatigue life x-axis, versus the fatigue life from the tests for the specimens without any significant flaws and $a_i = 0.1$. The left points indicated predictions done with mean +2SD parameters while the right points indicate predictions done with mean -2SD parameters.

The predictions based on $a_i = 0.1\text{mm}$ failed to accurately and conservatively predict the fatigue life of the specimens, the results failed with a similar offset for all the specimens on the log log-plot. For this reason another slightly higher initial crack length was used in a new set of predictions. This time $a_i = 0.5$ mm was used. The results from these predictions are displayed in figure 4.10. As the figure shows the tested fatigue life falls between the two extremes that the mean +2SD and mean -2SD represents, still the predictions are more to the non conservative side than to the conservative. Keeping in mind that a crack with a depth of 0.5 mm would at least need some % of cycles to initiate, a transition depth of 0.5 mm is still dubiously small, at least dubious for the condition these predictions are based on.

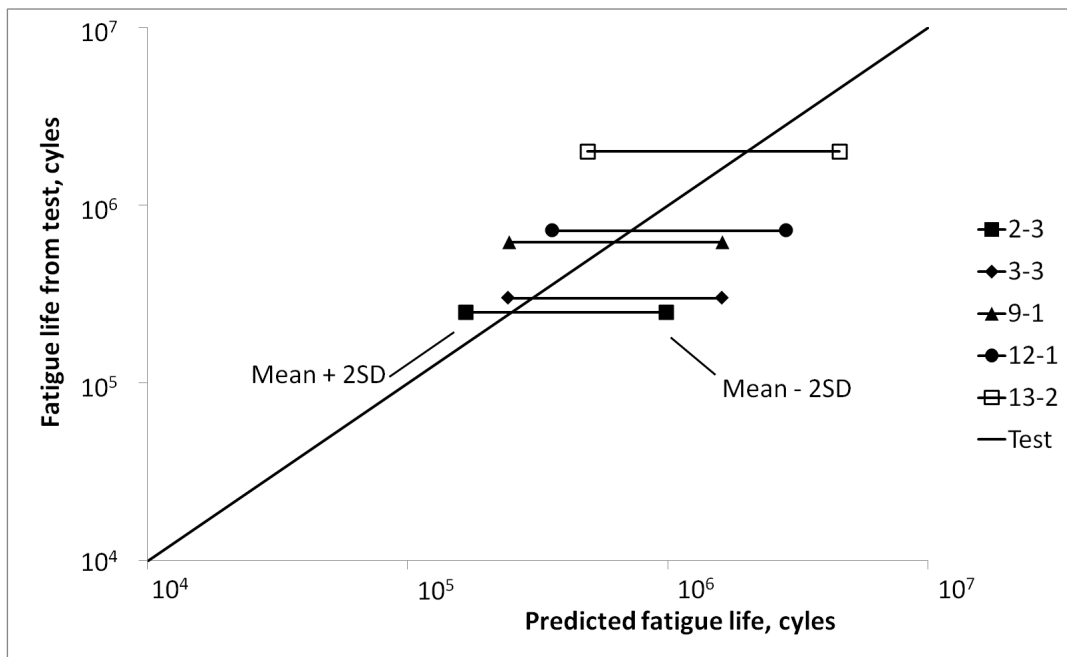


Figure 4.10: The figure illustrates the predicted fatigue life x-axis, versus the fatigue life from the tests for the specimens without any significant flaws and $a_i = 0.5$. The left points indicated predictions done with mean plus 2SD parameters while the right points indicate predictions done with mean minus 2 SD parameters.

4.2 DNV-RP-C203

4.2.1 Introduction

The design code DNV-RP-C203 [10] is DNV's recommended practice for fatigue design of offshore steel structures. This recommended practice includes guidelines for both design of low and high cycle fatigue. The design code is valid for steels in air with a yield strength below 900 MPa and for materials with yield strengths below 550 MPa for steels in maritime environment with or without cathodic protection. The main principle of the fatigue calculations in the design code is based on nominal $S-N$ curves. The design code covers a wide range of geometries, stress situations and different weld configurations. Which type of $S-N$ curve to use is based on factors such as, geometry, loading situation, weld type and weld quality. The $S-N$ curves have inherent failure criteria based on geometry and type of connection. For tubular joints the failure criterion is set to be crack growth through the thickness of the wall. The basic $S-N$ curve is given as:

$$\log(N) = \log\bar{a} - m\log\Delta\sigma, \quad (4.9)$$

where N is predicted number of cycles to reach failure criterion. $\Delta\sigma$ is the stress range, while m and $\log\bar{a}$ are the negative inverse slope of the $S-N$ curve and the intercept of the $S-N$ curve and $\log N$ axis. For welded joints the fatigue strength is somewhat dependent on plate or wall thickness. In DNV-RP-C203 this thickness effect is accounted for with the following modification of the $S-N$ curve:

$$\log(N) = \log\bar{a} - m\log\left(\Delta\sigma, \left(\frac{B}{B_{ref}}\right)^k\right) \quad (4.10)$$

In the equation above the B is the wall thickness of the wall or plate, B_{ref} is the reference thickness, while k is the thickness exponent. Since the wall thickness for the selected specimens was 20.9 mm and the reference thickness B_{ref} for girth welds is 25 mm. The equation 4.9 was used directly. DNV-RP-C203 includes two sets of m and $\log\bar{a}$ for each weld curve. For the $S-N$ curves in air it is one set for $N < 10^7$ and one set for $N > 10^7$. The design code also provides a fatigue limit for steel in air at 10^7 cycles. If the stress range in constant amplitude loading is lower than this limit, or no stress range in variable amplitude loading is greater than this limit, the design code predicts infinity life for the detail in question. The DNV-RP-C203 recommends no correction for the mean stress affect for welds due to residual stresses in welds. The reduction due to mean stresses is already included in the $S-N$ curves. Due to residual stresses the $S-N$ curves are comparable to $S-N$ curves with relative high mean stress, as discussed earlier. For regions of the detail that is not affected by residual stresses, and part of the stress range is in compression a reduction equation is proposed. All of the pipes from the selected data set were tested with $R = 0.1$. In other words none of the tested pipes were subjected to compressive stress. The areas of interest (the welds) did most likely include relative high tensile stresses. For these two reasons non corrections were made.

4.2.2 Fatigue life predictions of the selected specimens based on DNV-RP-C203

The S-N curves for the selected specimens from the JIP data base were D for the as welded connections and C1 for the ones which had ground flush welds. The parameters for the two design curves are given in table 4.3. To be consistent the nominal stress range was used and no correction for the small misalignment recorded in the test was used. A plot of the recorded life of the test data 3.1 versus the life predicted by use of

Table 4.3: S-N parameters for the S-N design curve C1 and D

S-N curve	$N < 10^7$ cycles	$N > 10^7$ cycles	Fatigue limit at 10^7
	$m_1 = 3$ $\log \bar{a}_1$	$m_2 = 5$ $\log \bar{a}_2$	cycles (<i>Mpa</i>)
C1	12.592	16.320	73.10
D	12.164	15.606	52.63

the equation 4.9 with the parameters value from table 4.3 are shown in figure 4.11. As can be seen in the same figure the design code underestimated the life for specimen 4, 6, 7 and 10. All the failed welds had flaws that affected the fatigue life. For the rest of the specimens the predictions based on the design code were conservative. Though S-N curves in general give conservative and reliable fatigue life predictions, this method is not very informative, except for the total fatigue life of the detail it does not provide much additional information. Information such as how an initiated crack will grow. This type of information is useful, especially when planning service intervals. In addition the predictions do not say anything regarding how many cycles it takes to initiate a crack.

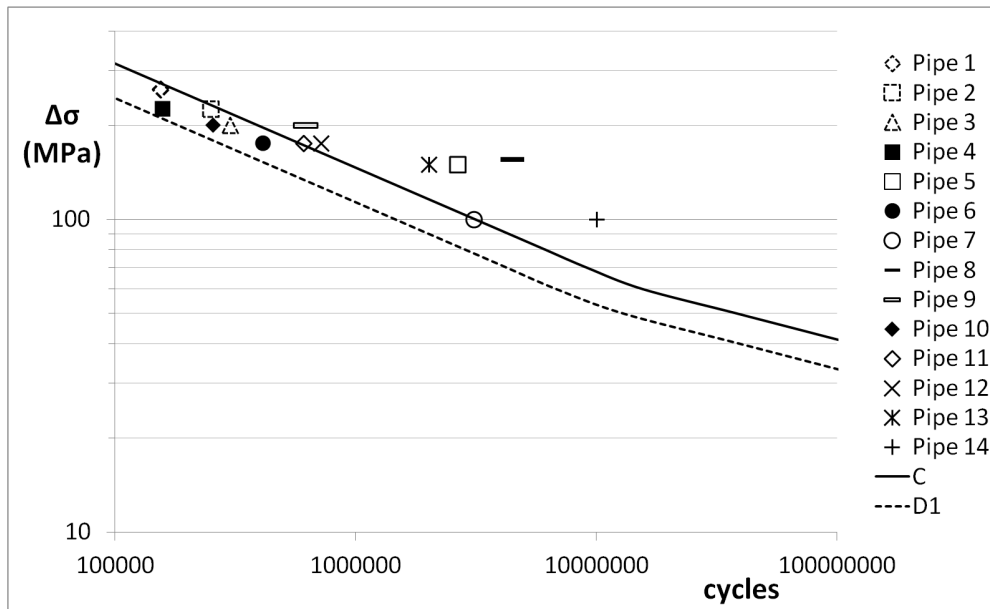


Figure 4.11: A plot showing recorded life and predicted life according to DNV-RP-C203. The dotted indicators and dotted curve refer to data with the S-N curve D respectively. The non-dotted indicators and curve refer to data with the S-N curve C1 respectively.

4.3 P-FAT

4.3.1 Introduction

P-FAT is a fatigue post processor tool. A post processor is program that uses information from a result, in this case a finite element analysis. This tool can be used to determine fatigue life both deterministic and probabilistic. The tool consists of several modules:

- Local stress module is (deterministic) life prediction based on the relationship between the highest stress point in a specimen and fatigue life of an equally stressed fatigue specimen.
- Single defect module is (deterministic) life prediction based on a crack like defect at the point of interest
- Weakest link module is (probabilistic) life prediction based on probability of survival of a component to be probability of survival of the components weakest element.
- Random defect module is (probabilistic) life prediction based the stress at a defect which position and size is obtained by uniform distribution and extreme value distribution respectively.

P-FAT uses the geometry and stresses extracted from a finite element analysis. The analysis could be performed in programs such as ABAQUS, ANSYS and NASTRAN. The result from a finite element analysis has to be converted into a .vtf file. This file is then loaded into P-FAT with the two P-FAT input files, before P-FAT can be run. The input files consist of the information P-FAT needed to run a simulation. One material file specifying the material properties and one file with the information on which module P-FAT should run and with which parameters to use. Single defect analyses (SDA) have been carried out on the load cases matching load cases the selected specimens were subjected to.

Single defect module

The single defect module uses the principal stresses extracted from a finite element analyse. It is possible to use different types of multiaxial stress criteria. The maximum principal stress criterion was used in the simulation of the fourteen specimens. This was done due to the fact that the simulations only included one uniaxial stress component, and the material properties such as yield strength or fatigue limit was not clearly specified for the material simulated. P-FAT includes two types of crack growth models. The first and the one used is based directly on the simple version of Paris law, the second a short crack model based on El Haddads intrinsic crack depth model [12]. P-Fat calculates the stress intensity factor by using weight functions. A weight function $w(p_i)$ is in fracture mechanics the stress intensity value given from a pair of unit opening forces at an arbitrary point p_i on the crack surface. To get the stress intensity for a crack one needs to integrate

the weight function and the crack face traction over the perimeter of the crack [2]:

$$K_I = \int_{\text{perimeter of crack}} p(x) w(x) dx \quad (4.11)$$

$p(x)$ is crack face traction is the normal stress that would act on the crack plane if there were no crack is present. The integral in equation 4.11 can be solved numerically. For an embedded crack P-FAT uses the following weight function [13]:

$$w(x, y, p) = \frac{\sqrt{2s}}{\pi^{3/2}\rho^2} \sqrt{1 - \frac{s}{8\rho_1} - \frac{s}{8\rho_2} - \frac{s}{8\rho_3} - \frac{s}{8\rho_4}} \quad (4.12)$$

In the equation above p is an arbitrary point on the crack surface while s is the shortest distance between the point s and the crack surface. ρ is the distance between the point p and the point on the crack surface where the stress intensity is to be determined. ρ_1 - ρ_4 are crack shape parameters. P-FAT calculates four stress intensities for an embedded crack. These four points A1, A2, C1 and C2 are displayed in figure 4.12. For the geometry of a pipe C1, and C2 will be equal. Wormsen [14] found good agreement between the use of weight functions and analytical solutions for stress intensity for embedded cracks. As long as $a/L \leq 0.9$ the recorded deviation between the two different solution were less than 4 %, L being the distance between the crack centre and the free surface as displayed in figure 4.12. When the crack grows through a free surface P-FAT recategorizes the embedded

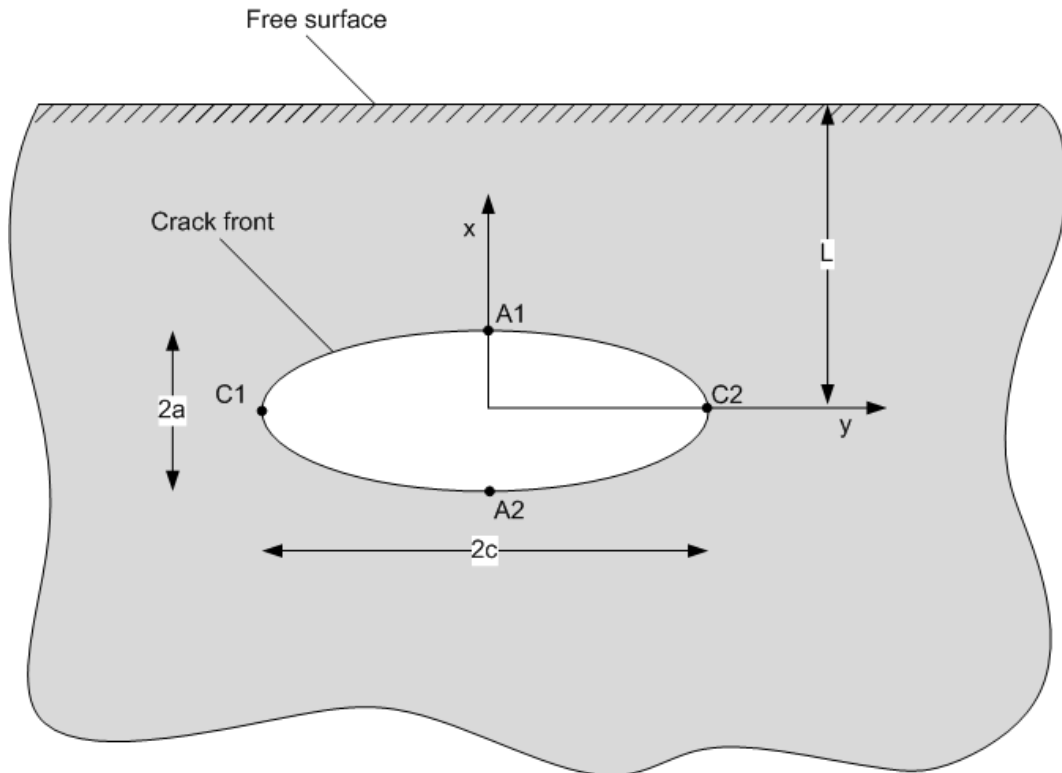


Figure 4.12: Illustration of an embedded crack with essential dimensions.

crack to a surface crack in the same manner as the BS7910 recommends. Setting the new crack depth a equal to $2 a$, while keeping the crack length c constant.

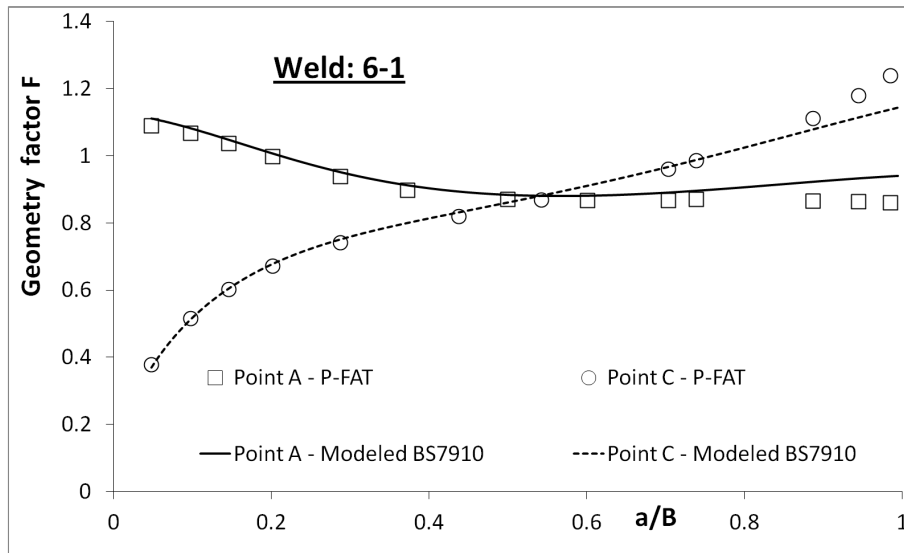
Surface crack

After re-categorizing the crack to a surface crack, two new weight functions are introduced. One weight function for the deepest point of the crack and one for the two points at the free surface. Wormsen [14] compared the stress intensity calculated by weight functions with finite element results found in literature. The deviation was found to be less than 4%. P-FAT let the crack grow further until the crack reaches a predetermined crack length, stress intensity value or the crack breaches the opposite free surface. P-FAT does not support through thickness cracks.

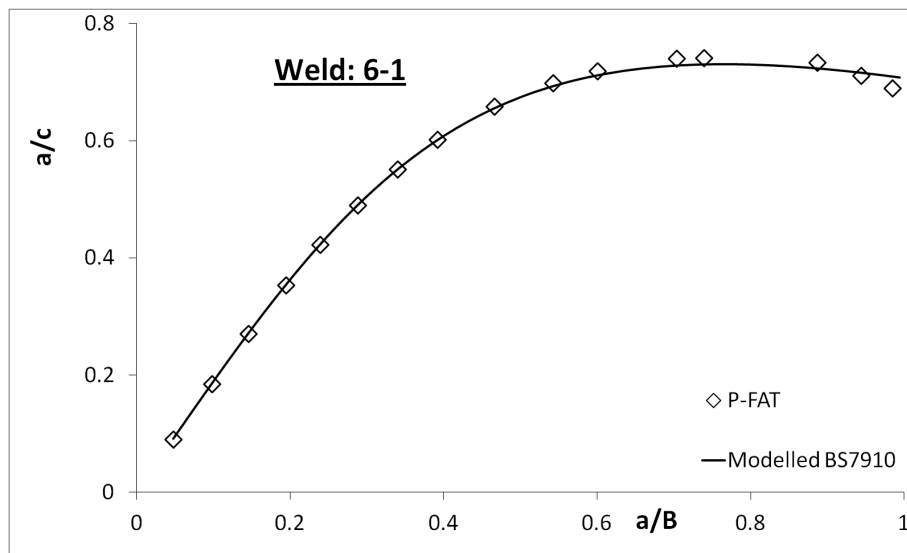
Validation of P-FAT

Prediction of fatigue life with P-FAT was performed on both the selected specimens that contained flaws and the specimens with no significant flaws. A comparison between the geometry factor F was made between the calculations from P-FAT and the calculations from the modelled BS7910. For cracks that had its origin as a surface crack only a small difference in the geometry factor F was noticeable between the modelled BS7910 and P-FAT. As figure 4.13 a) shows that the difference in geometry factor is small for weld 6-1 as the crack starts to grow, but as the crack grows closer to the free surface, the difference increases. A trend that is present for all thirteen welds is that the geometry factor estimated for the crack depth by P-FAT becomes lower than the one calculated by the modelled BS7910 as the crack grows. This indicates that P-FAT would predict longer fatigue lives than the modelled BS7910. The geometry factor for the crack length has the opposite trend for all thirteen welds. As figure 4.13 b) illustrates the the difference in geometry factor has little effect on the a/c relationship. Keeping in mind that weld 6-1 had an $a_i/c_i \leq 0.1$. For surface cracks with an $a_i/c_i = 1$, the behaviour of the geometry factor is similar as for the low a_i/c_i cases, but the difference in a/c deviates more at the maximum deviation which lies on $a/B \approx 0.7$. An opposite behaviour can be spotted for the surface cracks with low a_i/c_i and $a_i/c_i = 1$ respectively, while the difference in a/c is smaller for small a_i/c_i the difference in geometry factor is greater compared to $a_i/c_i = 1$. Still the deviations between the a/c relationships are relative small, and do roughly not exceed 5-6%. Plots for the a/c relationship and the geometry factor F can be found in appendix (reff appendix).

For cracks that had its origin as an embedded crack the recorded deviation for both a/c relationship and geometry factor was higher compared cracks that had its origin as a surface crack. Even though the modelled BS7910 and P-FAT give results that behave somewhat in the same manner, the deviations are larger. This is illustrated in figure 4.14. The deviation is still small for cracks that had its origin close to a free surface. The gaps that are visible in the plots represent the re-categorization of the crack, as it breaks through the free surface, and goes from being an embedded crack to becoming a surface crack. One reason for why the deviations in the results are greater for embedded cracks lies in the fact that the modelled BS7910 uses the same geometry factor for the points A1 and A2 in figure 4.12, while P-FAT uses two different geometry factors for these two locations. The two different geometry factors lead to that the amount crack growth in point A1 and A2 differ. The crack will grow faster in the point closest to the free surface, A1, than in point A2. This again makes the centre of the crack move closer to



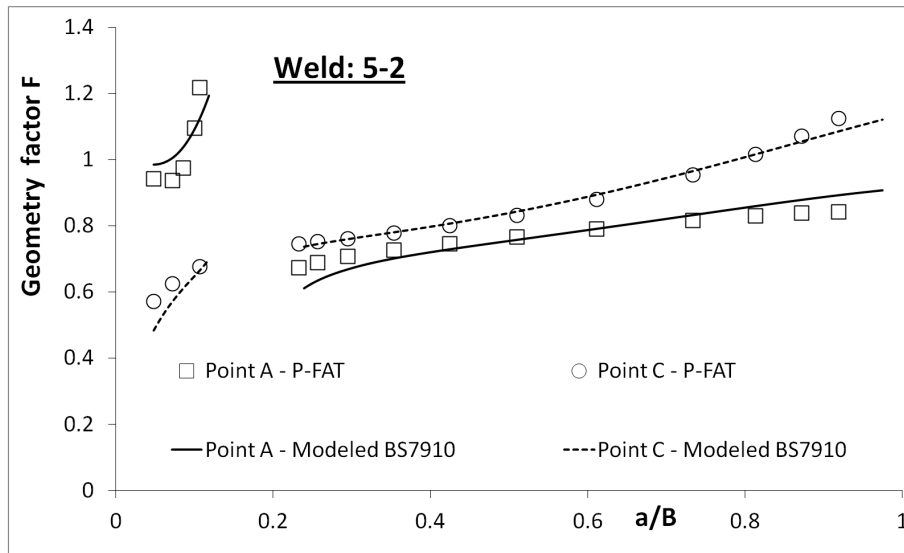
(a)



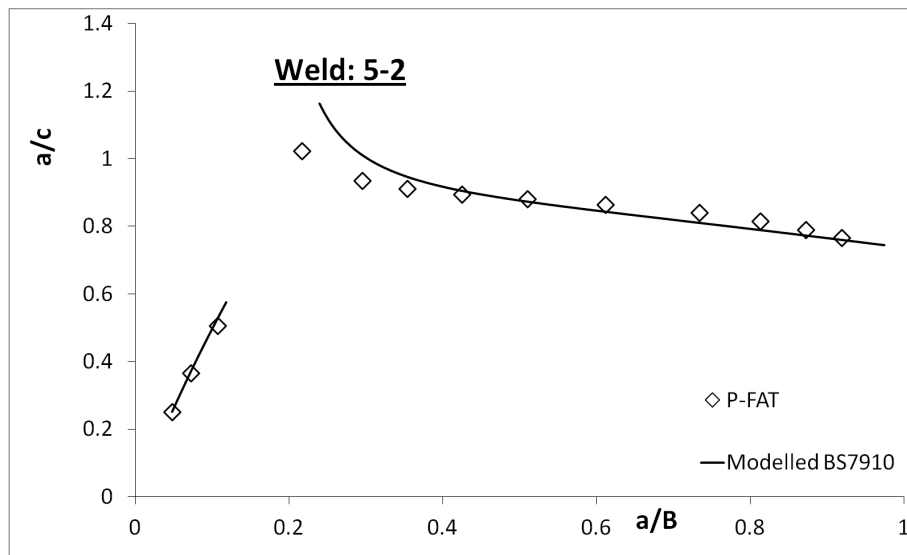
(b)

Figure 4.13: Figure a) illustrates the behaviour of the geometry factor in location A and C for weld 6-1 predicted by both P-FAT and the modelled BS7910, while figure b) illustrates the behaviour of the a/c relationship.

the surface as the crack grows and after the re-categorization the two different methods predict different crack depths a . The difference in crack depth a after re-categorization is denoted $\Delta a_{re-cat.}$. The two different behaviours are illustrated in figure 4.15. As the figure illustrates the two different methods have distinguished impacts on the a/c relationship, even if the geometry factor for point A1 is similar for the two methods. For weld 10-2 where the initial crack was located close to the centre of the wall thickness B , the effect of the different geometry factors used at point A1 and A2 in P-FAT is most obvious. The impact of the different geometry factors have on the a/c relationship is clearly visible in figure 4.16. Here the effect $\Delta a_{re-cat.}$ have on the re-categorized crack length can be seen.



(a)



(b)

Figure 4.14: Figure a) illustrates the behaviour of the geometry factor in location A and C for weld 5-2 predicted by both P-FAT and the modelled BS7910, while figure b) illustrates the behaviour of the a/c relationship.

4.3.2 Predicting fatigue life of the selected specimens with

The difference in the fatigue life predictions according to P-FAT and the modelled BS7910 have been compared. The parameters which have been used is the same as the life predictions done with the modelled BS7910 where the defect free a_i was set to 0.1 mm and the +2SD crack growth curve was used. The results are visible in table 4.4. As the table shows P-FAT predict longer fatigue lives compared to the modelled BS7910. A reason for this as mentioned earlier is the fact that the geometry factor for the crack depth is lower for the P-FAT calculations than for the BS7910. For embedded cracks the deviation in predicted fatigue lives is as high as 15%. One of the reasons for this is the

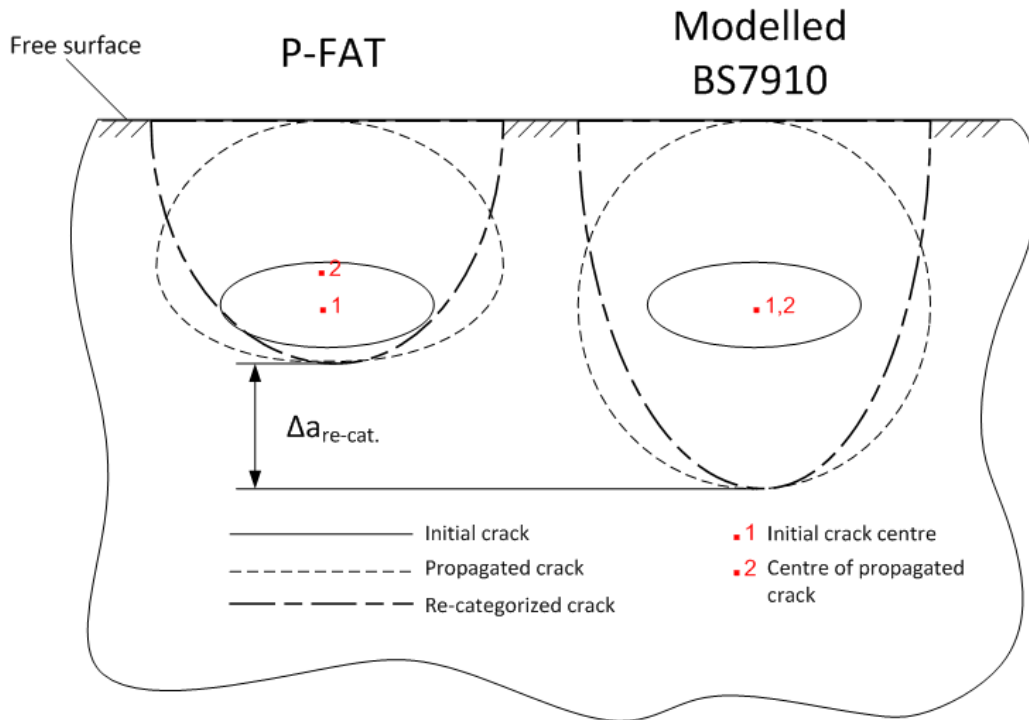


Figure 4.15: Figure illustrates the difference in behaviour behaviour of crack growth predicted by P-FAT and the modelled BS7910.

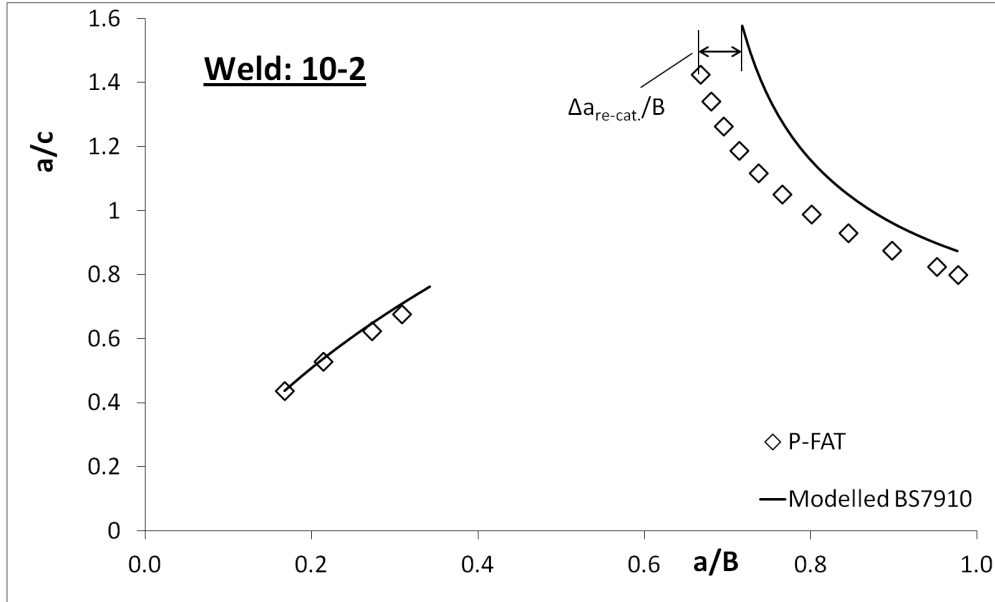


Figure 4.16: Illustrates the effect of P-FATs dual geometry factor for crack depth on the a/c relationship after the re-categorization of the crack.

as discussed above the fact that P-FAT uses two different geometry factors for A1 and A2, while the BS7910 just uses the same for both locations. Even though the highest geometry factor calculated by P-FAT is similar to the one calculated by the modelled BS7910, the other one is lower giving the $\Delta a_{re-cat.}$ after the crack has been re-categorized

to a surface crack. For the predictions done on cracks that had its origin as a surface crack the deviation is smaller. For weld 1-2 the deviation is 6.0 %. The a_i/c_i for this weld was quite extreme, compared to the other surface cracks. The rest of the surface cracks had all deviations under 3.5%.

Table 4.4: A comparison of number of fatigue cycles needed to grow the initial crack to a through crack for both P-FAT and the modelled BS7910.

Weld number	Type of initial crack	Modelled BS7910 Cycles to through crack	P-Fat Cycles to through crack	Difference in <i>per cent</i>
1-2	Surface	33616	35643	6.0
2-3	Surface	523756	536373	2.4
3-3	Surface	861414	885874	2.8
4-2	Embedded	23210	26600	15
5-2	Embedded	161138	181909	13
6-1	Surface	83994	87125	3.7
7-1	Embedded	342624	389864	14
8-1	Surface	526579	524261	0.4
9-1	Surface	861414	885874	2.8
10-2	Embedded	28808	30721	6.6
11-2	Surface	140668	142838	1.5
12-1	Surface	1563517	1612611	3.1
13-2	Surface	3240551	3310671	2.2

4.4 Two-Phase model

In this section a review of Lassen and Rechos two-phase model (TPM) will be done. There have not been performed any analyses with the model. The reason for this that material parameters needed to run this model was not available. An evaluation is done at the end of this chapter.

Lassen and Recho proposed in 2008 a two-phase model [15]. This model covers both the crack initiation phase of and subsequent growth of the crack. Hence the name TPM. The TPM calculates the total fatigue life N_{Tot} as:

$$N_{\text{Tot}} = N_i + N_p, \quad (4.13)$$

where N_i and N_p are respectively numbers of cycles to initiate the crack and the subsequent cycles of crack growth. Lassen and Recho tested made and tested this model on fillet welds. They assumed that most of the fatigue life was spent in the initiation phase. The initiation phase is modelled by local strain approach Coffin-Manson equation. Whereas the propagation phase are modelled after recommendations given by BS 7910 by means of the Paris law for a 2D stress situation. The TPM was fitted to experimental data for crack growth histories for two databases. The Numbers of cycles to initiation N_i are based on the Coffin-Manson equation with Morrows mean stress correction :

$$\frac{\Delta\varepsilon}{2} = \frac{(\sigma'_f - \sigma_m)}{E} + (2N_i)^b + (2N_i)^c \quad (4.14)$$

Where $\Delta\varepsilon$ is the local strain range and σ_m is local mean stress. The b and c are respectively the fatigue strength and the ductility exponents. The Ramberg-Osgood cyclic strain curve gives the local stress and strain relationship:

$$\Delta\varepsilon = \frac{\Delta\sigma}{E} + 2\left(\frac{\Delta\sigma}{2K'}\right)^{\frac{1}{n'}} \quad (4.15)$$

Here K' and n' are respectively the cyclic strength coefficient and the strain hardening exponent . The last equation is combined with Neublers rule:

$$\Delta\varepsilon\Delta\sigma = \frac{(K_t\Delta S)^2}{E} \quad (4.16)$$

where ΔS is the remote stress and E and K_t are respectively the Youngs modulus and the stress concentration factor. A problem with determining the stress concentration factor is that it varies along the weld seam. Lassen and Recho used an extreme value distribution to indentify the most likely smallest radius along the weld seam. As mentioned earlier defining a transition depth has been somewhat arbitrarily done in the fatigue community. Lassen and Recho choose a depth of 0.1mm. They supported this decision with the three arguments:

- It is questionable to apply fracture mechanics models to cracks with depths that approaches the grain size
- The difficulties with measuring cracks with depths less than 0.1 mm by means of non destructive examination with any accuracy, even for laboratory tests

Table 4.5: Results found by Lassen and Recho with the TPM.

Stress range (MPa)	Ni (cycles) TMP	Np (cycles) TMP	Nt (cycles) TMP	Nt F-class (BS5400)
150	1.4E5	3.3E5	4.7E5	5.1E5
120	5.6E5	6.5E5	1.2E6	1E6
100	2.1E6	1.1E6	3.2E6	1.7E6
80	1.6E7	2.2E6	1.8E7	3.4E6

- Cracks with depths less than 0.1 mm are not of interest in in-service inspections.

To determine the parameters for the Coffin-Manson equation Lassen and Recho calibrated the parameters for the Coffin-Manson equation by the following relationship based on Brinell hardness (BH):

$$\begin{aligned}
 S_u &= 3.45HB \\
 S'_y &= 0.608S_u \\
 b &= -0.1667 \log \left(2.1 + \frac{917}{S_u} \right) \\
 c &= -0.7 < c < -0.5 \\
 n' &= \frac{b}{c} \\
 K' &= S_y(0.002)^{-n'} \\
 \sigma'_f &= 0.95S_u + 370 \\
 \varepsilon'_f &= \left(\frac{\sigma'_f}{K'} \right)^{\frac{1}{n'}}
 \end{aligned} \tag{4.17}$$

Where S_u, S_y and S'_y are tensile stress, yield stress and cyclic yield stress respectively. Using HB as a governing variable is not exact. Lassen and Recho used this relationship, with a fitted HB value to get the parameters to fit the 0.1 mm initiation time. The BH they found was only 5% lower than the maximum value they got from hardness tests on the HAZ. Some of the results found by Lassen and Recho is displayed in table 4.5 Lassen and Recho raise the question if the extra work in estimating the fatigue life by means of the TPM is worth the extra work this model requires, compared to the relative simple way of doing it with help from the standard and guidelines as shown in the previous sections. They argue that in cases where inspections are planned to be carried out, the TPM would be to great help. This because the TPM gives an indication on when the crack has reached a detectable depth in addition to the fatigue life, and therefore indicated when inspection is needed.

The results displayed in Lassen and Rechos paper is promising, since the model gives the opportunity to calculate both the initiation time as well as the total fatigue life. As Lassen and Recho themselves suggests, future work should be carried out on different welding configurations such as butt joints. It would be interesting to see if the TPM is robust enough to accurately handle different configuration. If this is a fact the TPM can prove to be an important tool for the engineers in the future.

4.5 Discussion on the fatigue life prediction models

The different methods have been discussed to some extent in the previous sections. A somewhat more thorough discussion and comparison will take place here. The complete fatigue life prediction done with the recommended practice DNV-RP-C203 is a relative simple and reliable way to do fatigue assessments of welded components. The results gained from the predictions done in section 4.2 gave conservative and correct prediction for most of the test specimens. It failed to conservatively predict the fatigue life of four of the flawed specimens. The $S-N$ curves method have no good way to handle cases where flaws of significant size are present. Such a method could perhaps be implemented, but it would be rather unpractical. In any case where inspection are planned to be carried out the method is somewhat insufficient. The $S-N$ provide no information on expected crack growth during the last part of the fatigue life. Therefore cannot be used to assess the acceptability of an growing fatigue crack. The use of $S-N$ curves will still be an important method to predict fatigue life in the, due to the fact that the method is relative easy and reliable.

The modelled BS7910 assessed in section 4.1 gave results in good agreement with results from CrackWise, for surface and embedded cracks. A deviation was observed for through cracks. The modelled version was still found to deliver acceptable results, under the assumption that the fatigue cracks from the experimental result spent most of their fatigue life as embedded or/and surface cracks. The fatigue life prediction for the flawed specimens gave conservative results but still in agreement with results from the experimental data. The prediction with the parameters from the mean +2SD crack growth curve gave results close to the experimental results. A reason for the prediction being located close to the conservative +2SD predictions, is perhaps that it might be too conservative assess flaws as cracks or that the idealization of the flaw shape is conservative for some flaw shapes.

For the specimens without any significant flaws at the initiation point for the main fatigue crack, the $a_i = 0.1mm$ gave non conservative predictions. The predictions were conservative even for parameters for the mean + 2SD crack growth curve. A $a_i = 0.5mm$ was used, and gave predictions within the distributions of the crack growth rate curves used. If any additional initiation time were to be added upon the fatigue life predicted, a transition depth of 0.5 mm is still dubious. At least for the assumptions made in this thesis. This topic recommended for more thorough examination. If the predictions from the modelled BS7910 are compared with the predictions from the recommended practice, it can be sad that the fatigue crack grow model that BS7910 represents are suitable to assess components containing known flaws. The recommended practice failed to do so.

The use of P-FAT described in section 4.3 to assess fatigue crack growth and life prediction, gave comparable results to the modelled BS7910. This is perhaps not so strange since the BS7910 allows for weight functions to be used to assess crack growth. For most of the specimens the difference in fatigue cycles was small, but for embedded cracks a higher deviation was noticed. This is most likely related to the fact that P-FAT uses two different stress intensity factors in the crack depth direction while the modelled BS7910 uses just one. This involves that the centre of the embedded crack predicted P-FAT will move closer to the surface as the crack grows. As the crack breaks the surface the new re categorized crack depth will differ for the two different methods. P-FAT and

CrackWise have both strengths and weaknesses if the two assessment tools are compared. P-FAT uses the stress components extracted from a finite element analysis, this makes it necessary to perform such an analysis to perform a fatigue assessment, while CrackWise does not require such an analysis. Because a finite element analysis is time consuming the CrackWise is preferable. For the same reason P-FAT could be said to be preferable, because CrackWise is limited to the loading cases specified in the BS7910 standard. P-FAT can be run on different geometries with a wider spectre of loading cases, which can be preferable. In addition P-FAT automatically re-categorizes an embedded crack that penetrates a free surface, while CrackWise in these cases terminates the ongoing analysis.

The results presented by Lassen and Recho on the two phase model are seemingly promising reviewed in section 4.4, but there are some element of uncertainty for the model to be used on other configurations than fillet welds, such as an girth weld. One is that the stress concentration factor K_t for fillet welds might be more pronounced for fillet welds than for butt welds. How does the model work for configurations with relatively low stress concentration factor? A relatively low K_t raises another problem. Since the K_t might be higher for fillet welds, with a locus at the weld toe. The highest K_t for at least grinded butt welds might be located sub surface at an internal defect. If this is the case, the types, sizes and locations of these defects are needed. Secondly a K_t for the critical defect needs to be established based on type, size and shape. This will almost impossible, nor practical for defects of irregular shape such as lack of fusion defects. As mentioned earlier the transition depth of 0.1 mm suggested by Lassen and Recho, is dubious for the loading cases presented in this thesis. At least for the assumptions made. Perhaps another transition depth is required for girth welds. All these questions need answering before the model can be applied to other configurations than the fillet weld.

Chapter 5

Conclusion

Predictions of fatigue life in large girth welded pipes have been performed. A version based on BS7910 have been modelled up and verified against the fatigue assessment tool CrackWise. Both tools gave matching results for embedded and surface cracks. They did however give different results for through cracks. The modelled version was still found to give acceptable results. Fatigue life predictions were then performed with the modelled version on load cases matching load cases from experimental data. Good agreement was found between the predicted fatigue life and the experimental results for the specimens that contained flaws of significant size. When the initial crack depth was set to 0.1 mm the modelled version predicted non conservative results for the specimens that did not have significant flaws. A initial crack depth of 0.5 mm used in a later prediction on the same load cases, and gave acceptable results. The initial crack depth of 0.5 mm was still found dubious, because little tolerance was given for crack initiation to the 0.5 mm crack depth. The results gained from the modelled version were compared with results from the fatigue assessment tool P-FAT. The results from both the tools showed good agreement, though some deviation was found for embedded cracks. The design curves from DNV-RP-C203 showed good agreement for most of the load cases, but failed to conservatively predict the fatigue life for the welds that contained flaws.

A two-phase model developed for fillet welds have been reviewed. The results from presented in the literature a promising. But to apply the model on different welded configuration further investigating is need.

5.1 Future work

It is recommended that further investigation of fatigue life prediction of embedded cracks by P-FAT is conducted. This to make sure the results from crack growth predictions on embedded cracks matches experimental result.

To be able to apply the two-phase model on girth welds, it is recommended that investigation on the transition depth are performed. As well as investigations on whether the strained based approach used to predict the initiation cycles are suitable to asses welds with low stress concentration factor.

Bibliography

- [1] S. Suresh, *Fatigue of materials*. Cambridge University Press, 1st paperback ed. (with corrections and exercises) ed., 1992.
- [2] T. L. Anderson, *Fracture Mechanics: Fundamentals and Applications, Third Edition*. CRC Press, 3 ed., 5 2004.
- [3] N. E. Dowling, *Mechanical Behavior of Materials*. Pearson International, 2007.
- [4] T. Lassen and N. Recho, *Fatigue life analyses of welded structures*. Wiley Online Library, 2006.
- [5] C. Radaaj, D. Sonsino and W. Fricke, *Fatigue assessment of welded joints by local approaches*. Woodhead publishing, 2006.
- [6] D. . P. P. Askeland, *The science and engineering of materials*. Nelson, student edition ed., 2006.
- [7] J. R. Rice, “Dislocation nucleation from a crack tip: An analysis based on the peierls concept,” *Journal of the Mechanics and Physics of Solids*, vol. 40, no. 2, pp. 239 – 271, 1992.
- [8] P. Hansson and S. Melin, “Dislocation-based modelling of the growth of a microstructurally short crack by single shear due to fatigue loading,” *International Journal of Fatigue*, vol. 27, no. 4, pp. 347 – 356, 2005.
- [9] S. Kalpakjian and S. Schmid, *Manufacturing, Engineering & Technology (5th Edition)*. Prentice Hall, 5 ed., 8 2005.
- [10] “Recommended practice dnv-rp-c203 fatigue design of offshore structures,” April 2010.
- [11] Y. Murakami, *Stress intensity factors handbook*, vol. 2. Pergamon Press, 1987.
- [12] M. E. Haddad, T. Topper, and K. Smith, “Prediction of non propagating cracks,” *Engineering Fracture Mechanics*, vol. 11, no. 3, pp. 573 – 584, 1979.
- [13] G. Shen and G. Glinka, “Weight functions for a surface semi-elliptical crack in a finite thickness plate,” *Theoretical and Applied Fracture Mechanics*, vol. 15, no. 3, pp. 247 – 255, 1991.
- [14] A. Wormsen, A. Fjeldstad, and G. H. rd, “A post-processor for fatigue crack growth analysis based on a finite element stress field,” *Computer Methods in Applied Me-*

chanics and Engineering, vol. 197, no. 6 8, pp. 834 – 845, 2008.

- [15] T. Lassen and N. Recho, “Proposal for a more accurate physically based sn curve for welded steel joints,” *International Journal of Fatigue*, vol. 31, no. 1, pp. 70 – 78, 2009. `ice:title;Fatigue assessment of welded connections;ce:title;`.
- [16] “Bs7910:2005 guide to methodes for assessing the acceptability of flaws in metallic structures,” July 2005.

Appendix A

Comparison of geometry factor F for the modelled BS7910 and CrackWise

In this appendix all plots for the normalized geometry factor for all the configuration of a_i/c_i found in table 4.1 are found together with the normalized geometry factor for the through crack with initial length of $c = 5\text{mm}$.

A.1 Surface cracks

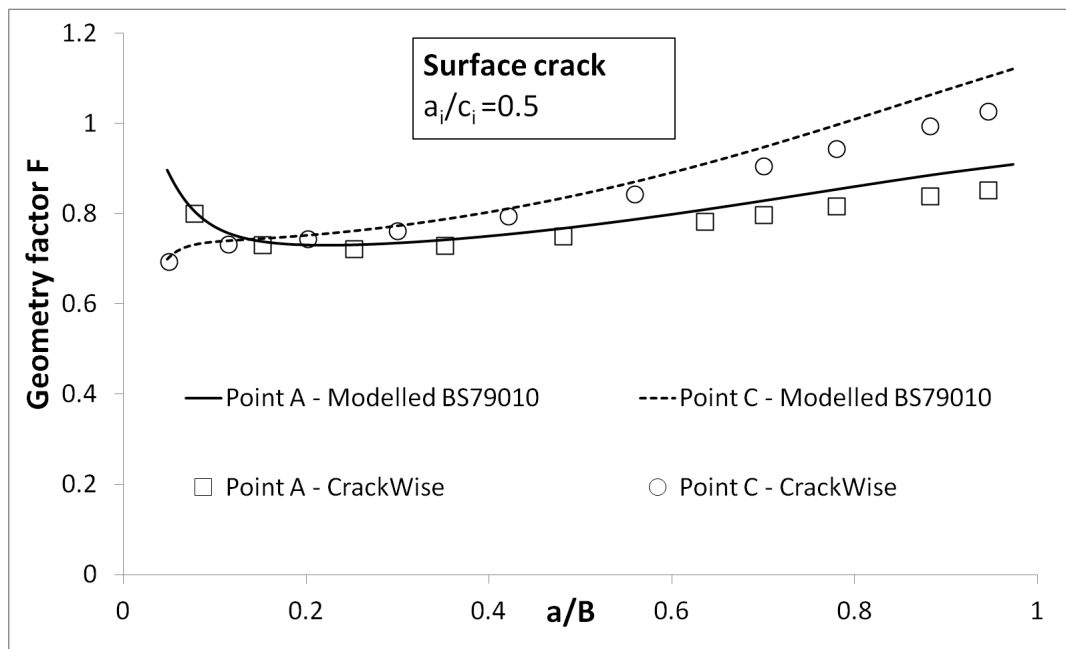


Figure A.1: Geometry factor as the crack grows for calculations done by the modelled BS7910 and CrackWise for a surface crack with initial a_i/c_i ratio of 0.5.

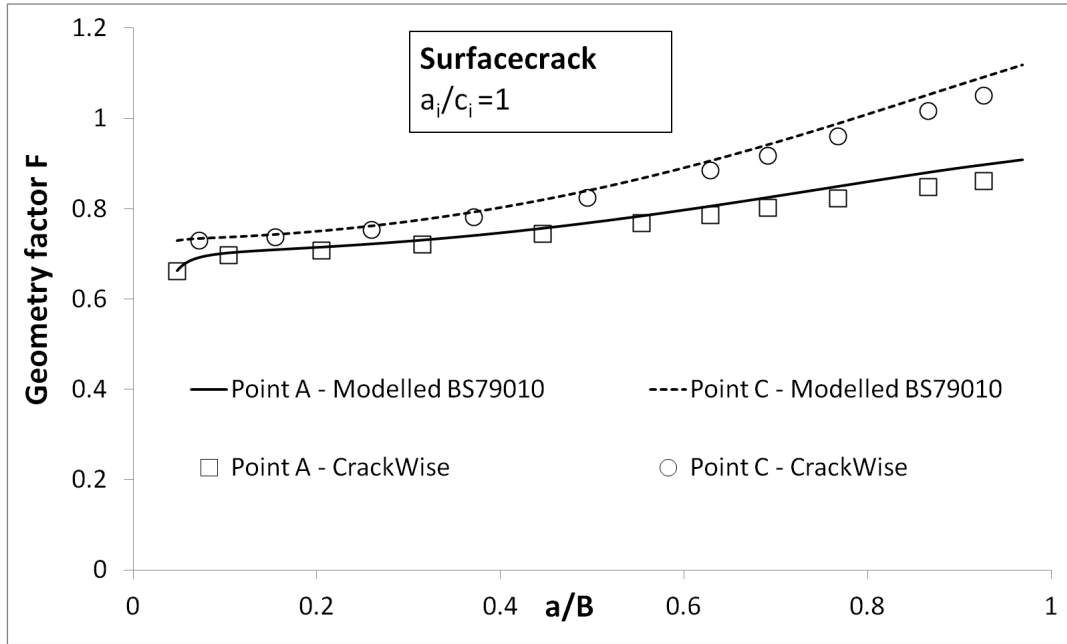


Figure A.2: Geometry factor as the crack grows for calculations done by the modelled BS79010 and CrackWise for a surface crack with initial a_i/c_i ratio of 1.

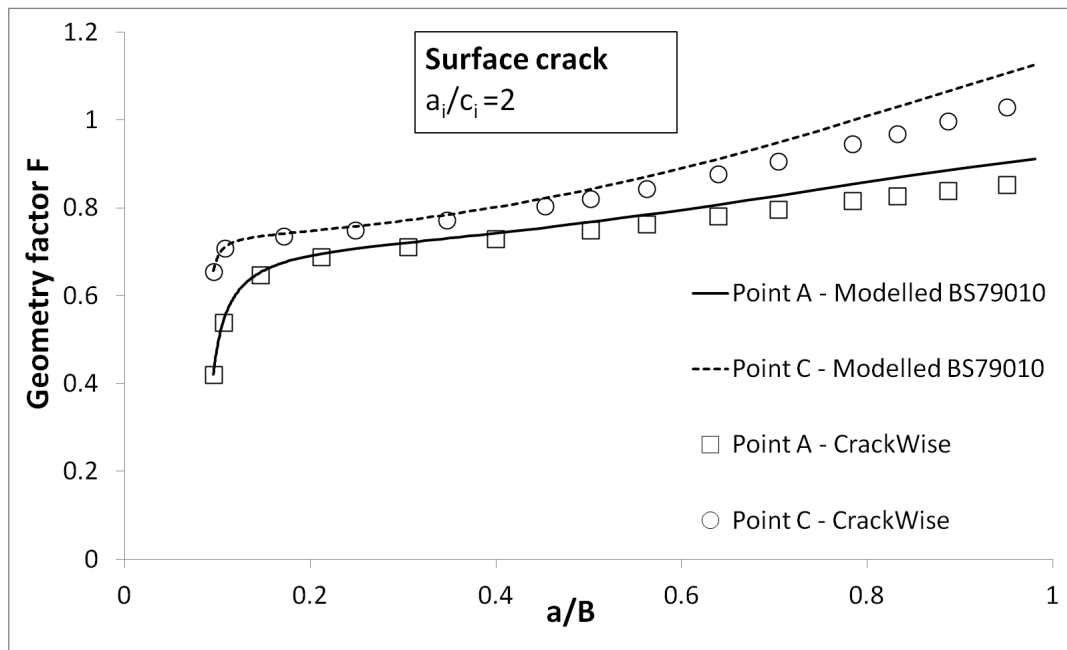


Figure A.3: Geometry factor as the crack grows for calculations done by the modelled BS79010 and CrackWise for a surface crack with initial a_i/c_i ratio of 2.

A.2 Surface cracks

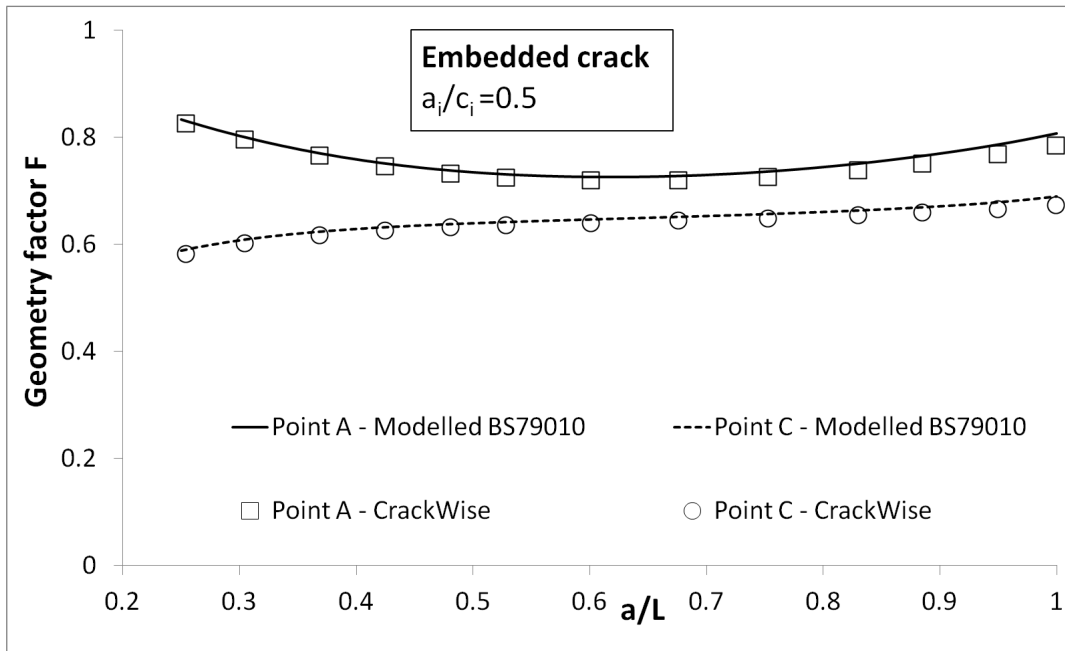


Figure A.4: Geometry factor as the crack grows for calculations done by the modelled BS79010 and CrackWise for a surface crack with initial a_i/c_i ratio of 0.5.

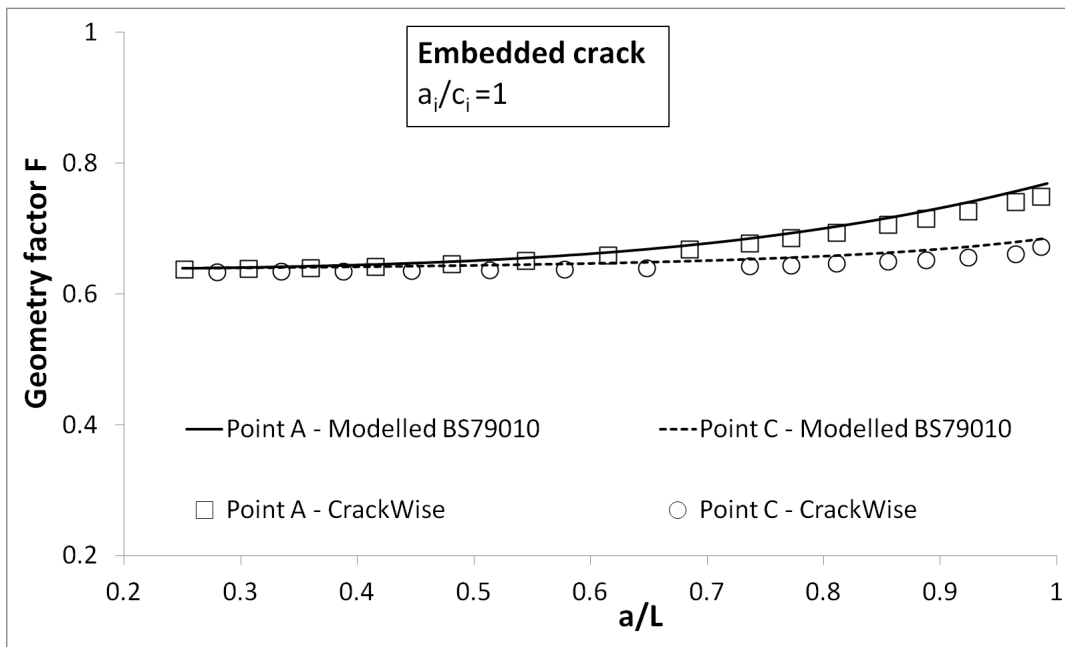


Figure A.5: Geometry factor as the crack grows for calculations done by the modelled BS79010 and CrackWise for a surface crack with initial a_i/c_i ratio of 1.

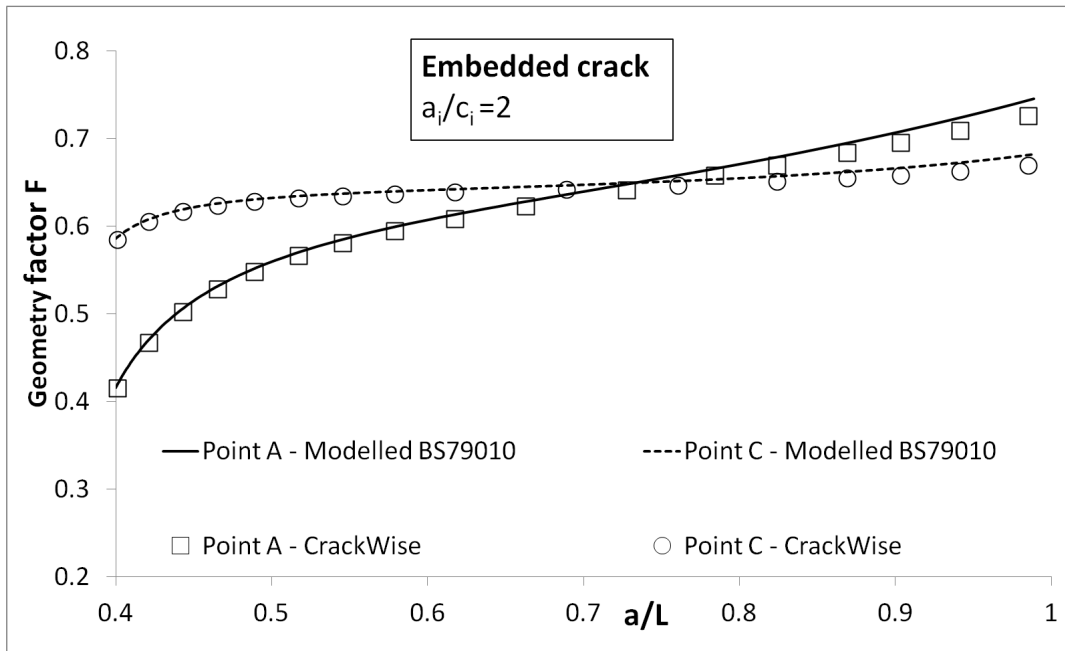


Figure A.6: Geometry factor as the crack grows for calculations done by the modelled BS7910 and CrackWise for a surface crack with initial a_i/c_i ratio of 2.

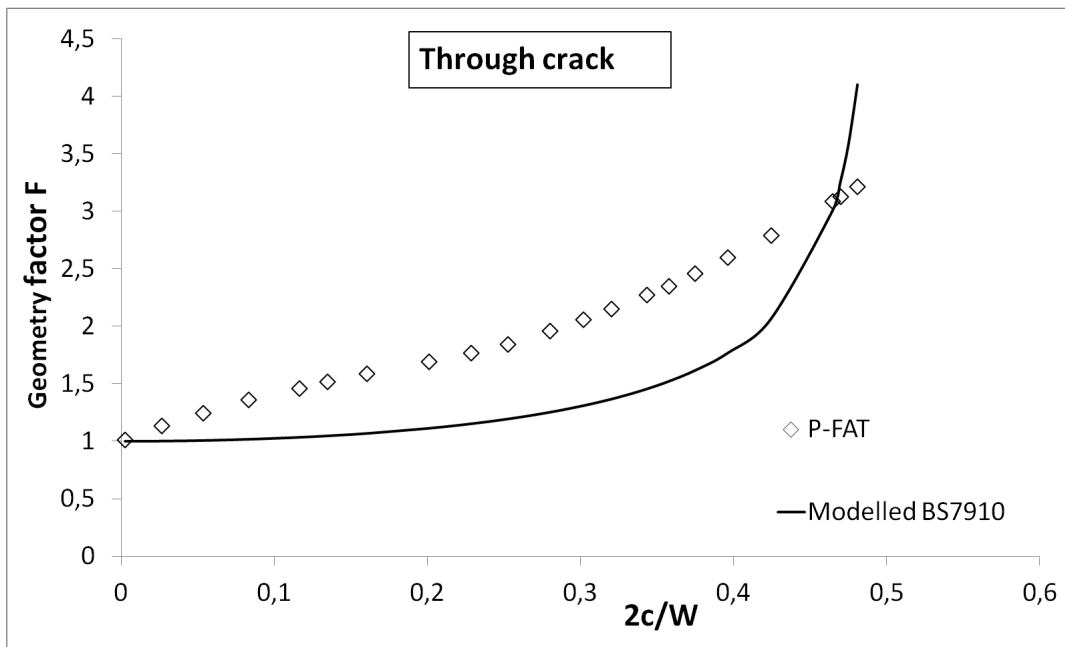
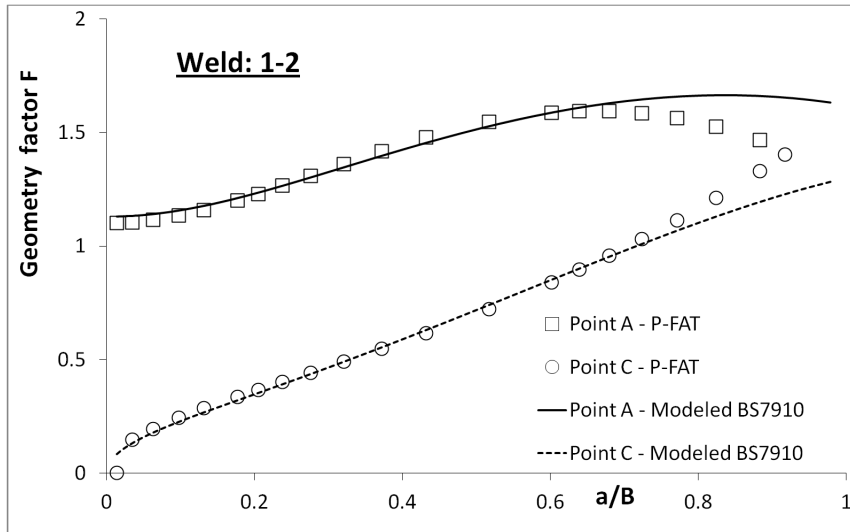


Figure A.7: Geometry factor as the crack grows for calculations done by the modelled BS7910 and CrackWise for a surface crack with initial a_i/c_i ratio of 2.

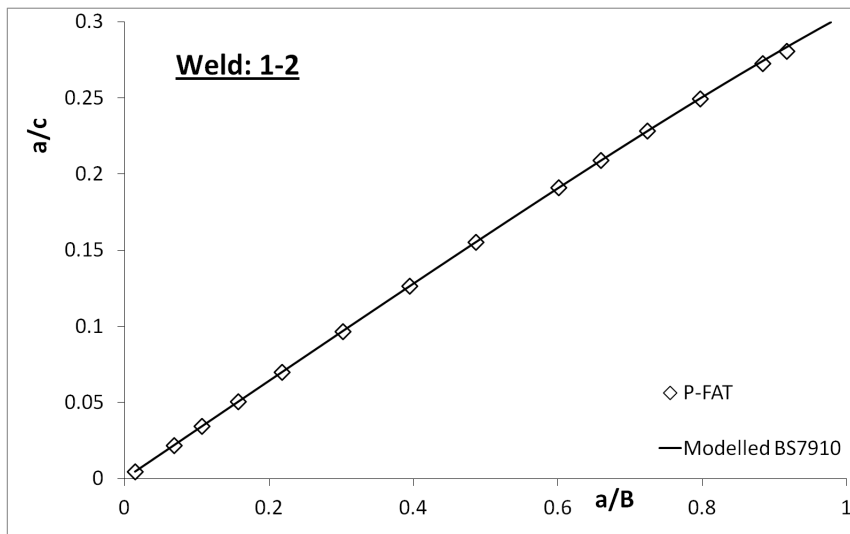
Appendix B

Comparison of geometry factor F and a/c for the modelled BS7910 and P-FAT

This appendix contains normalized plots for both the geometry factor F and the a/c relationship for the thirteen welds that failed, calculated by BS7910 and P-FAT

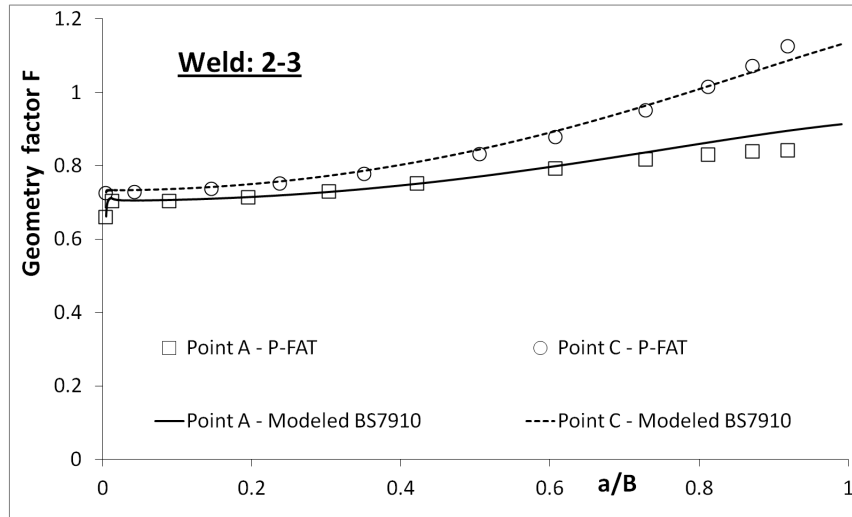


(a)

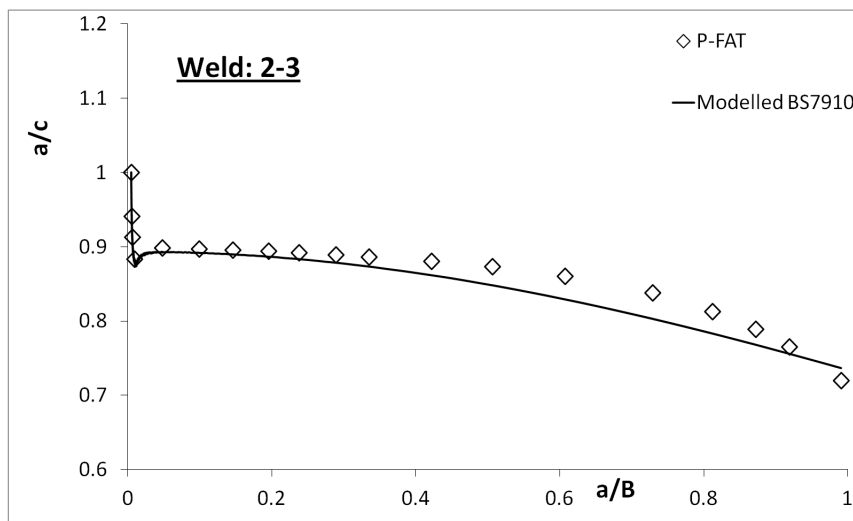


(b)

Figure B.1: Figure a) illustrates the behaviour of the geometry factor in location A and C for weld 1-2 predicted by both P-FAT and the modelled BS7910, while figure b) illustrates the behaviour of the a/c relationship.

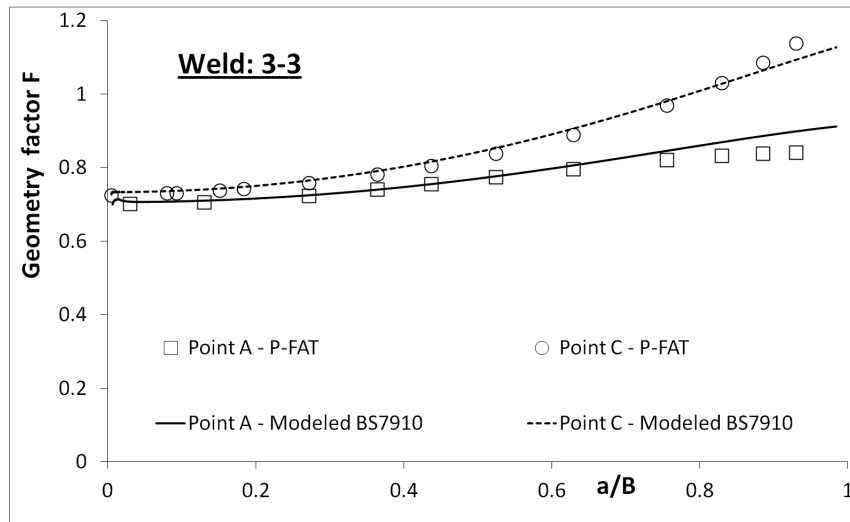


(a)

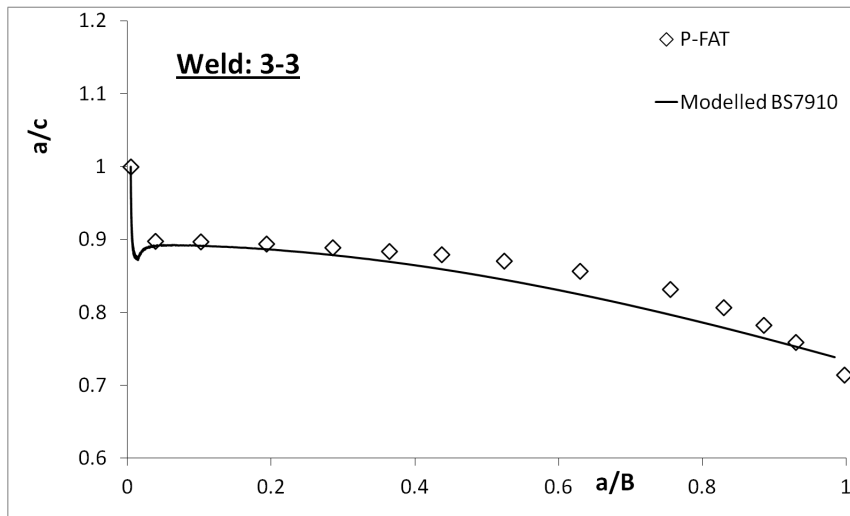


(b)

Figure B.2: Figure a) illustrates the behaviour of the geometry factor in location A and C for weld 2-3 predicted by both P-FAT and the modelled BS7910, while figure b) illustrates the behaviour of the a/c relationship.

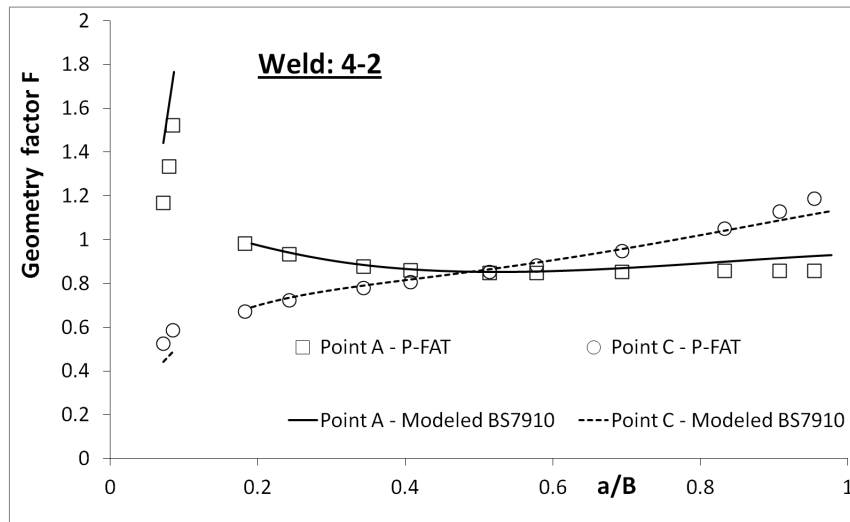


(a)

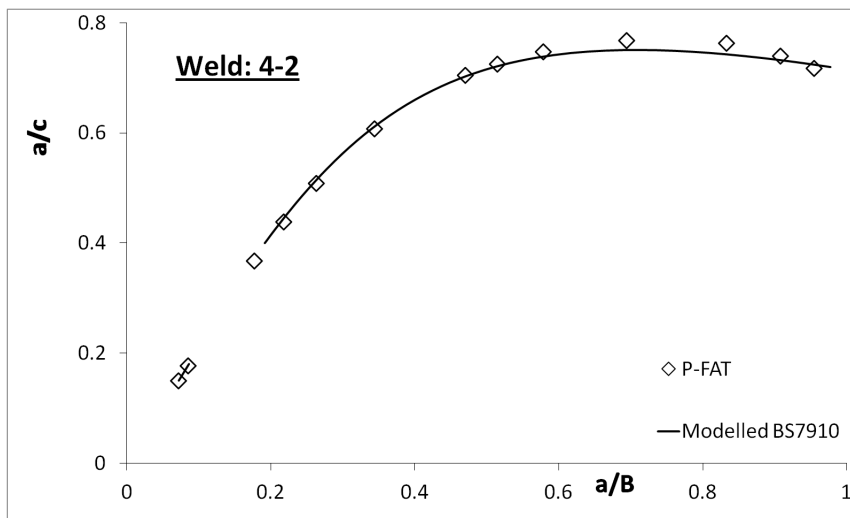


(b)

Figure B.3: Figure a) illustrates the behaviour of the geometry factor in location A and C for weld 1-2 predicted by both P-FAT and the modelled BS7910, while figure b) illustrates the behaviour of the a/c relationship.

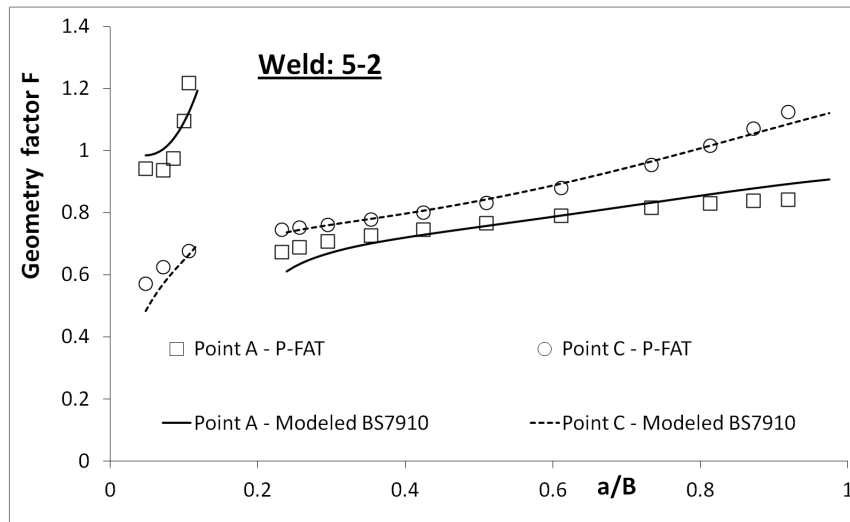


(a)

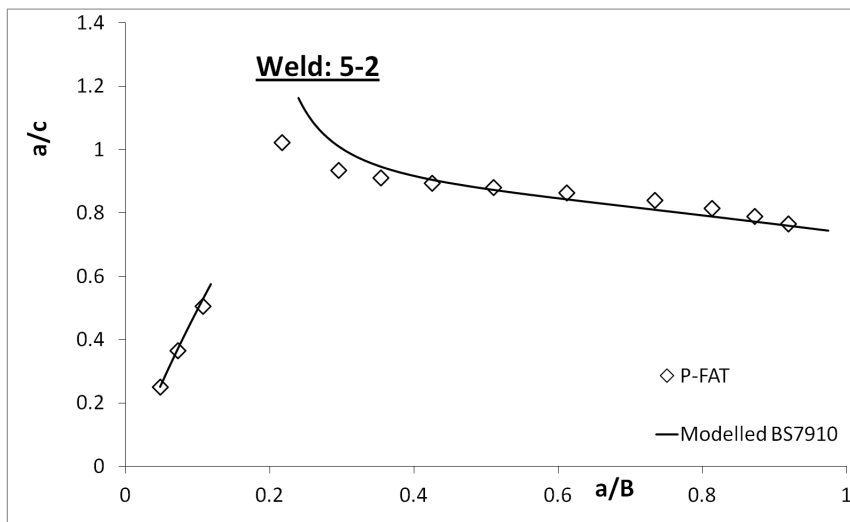


(b)

Figure B.4: Figure a) illustrates the behaviour of the geometry factor in location A and C for weld 4-2 predicted by both P-FAT and the modelled BS7910, while figure b) illustrates the behaviour of the a/c relationship.

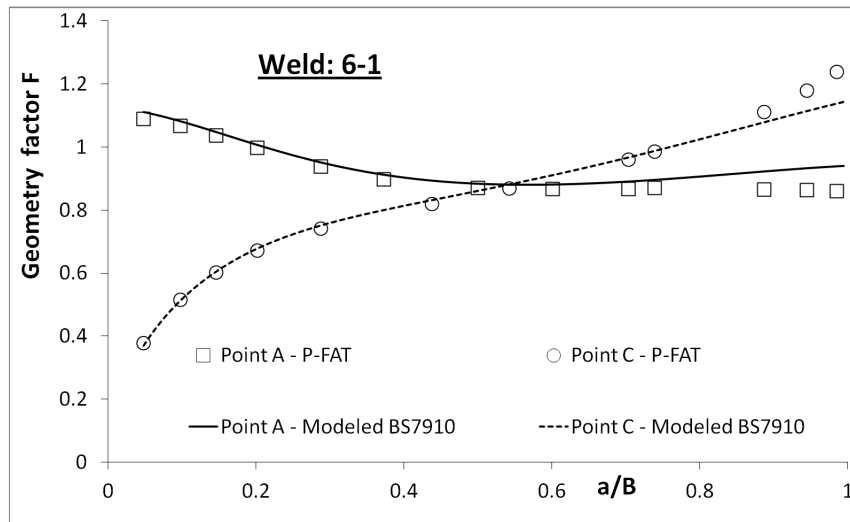


(a)

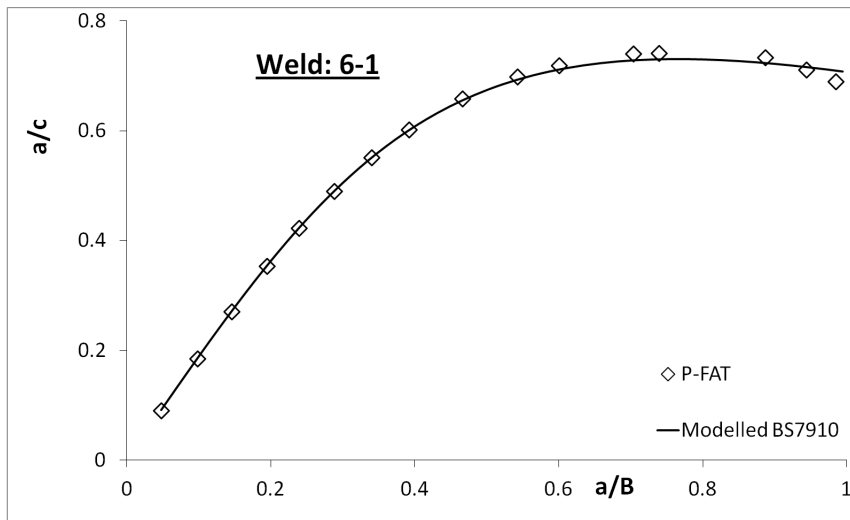


(b)

Figure B.5: Figure a) illustrates the behaviour of the geometry factor in location A and C for weld 5-2 predicted by both P-FAT and the modelled BS7910, while figure b) illustrates the behaviour of the a/c relationship.

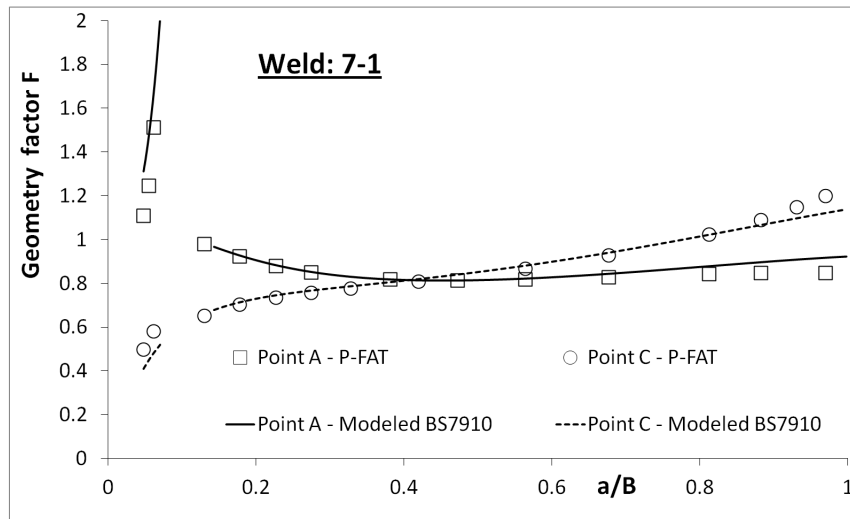


(a)

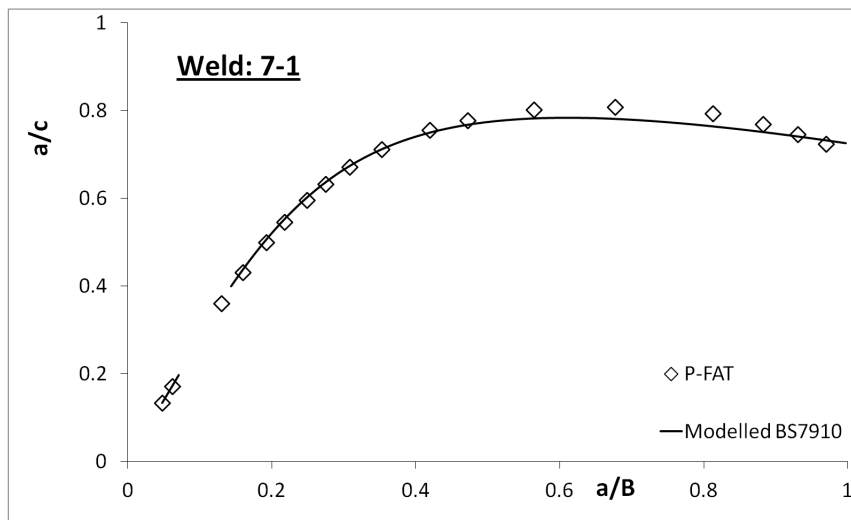


(b)

Figure B.6: Figure a) illustrates the behaviour of the geometry factor in location A and C for weld 6-1 predicted by both P-FAT and the modelled BS7910, while figure b) illustrates the behaviour of the a/c relationship.

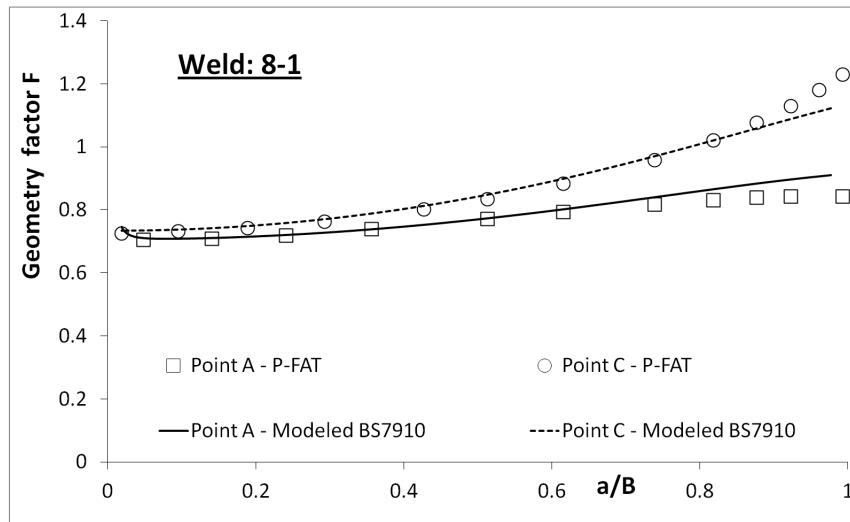


(a)

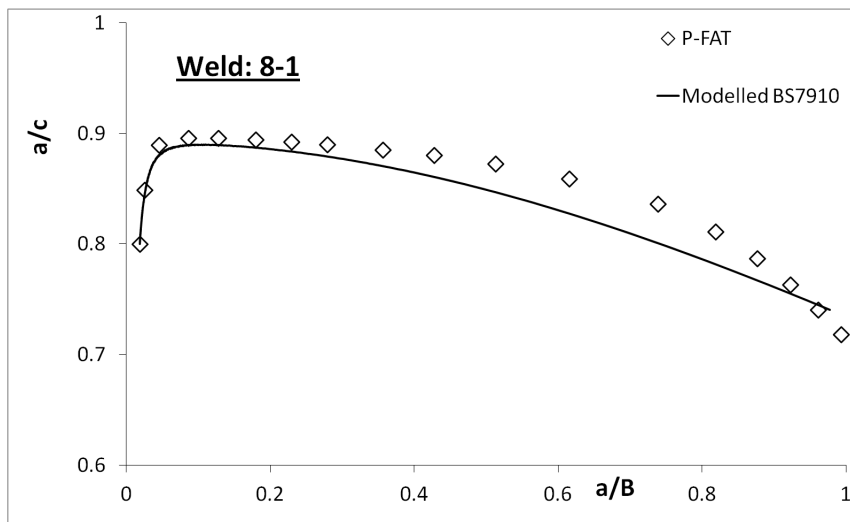


(b)

Figure B.7: Figure a) illustrates the behaviour of the geometry factor in location A and C for weld 7-1 predicted by both P-FAT and the modelled BS7910, while figure b) illustrates the behaviour of the a/c relationship.

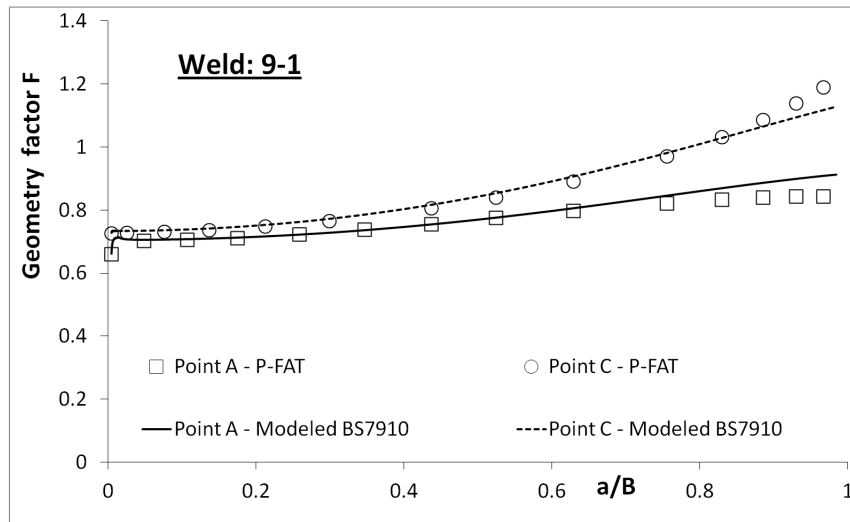


(a)

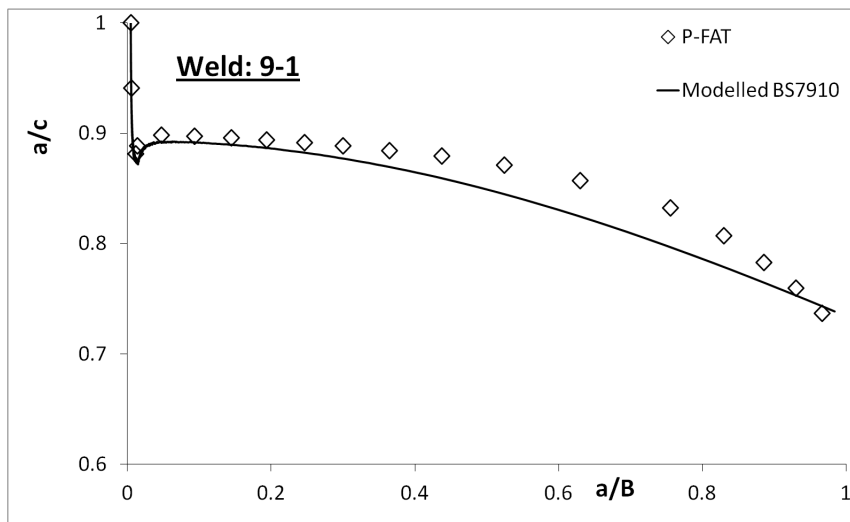


(b)

Figure B.8: Figure a) illustrates the behaviour of the geometry factor in location A and C for weld 8-1 predicted by both P-FAT and the modelled BS7910, while figure b) illustrates the behaviour of the a/c relationship.

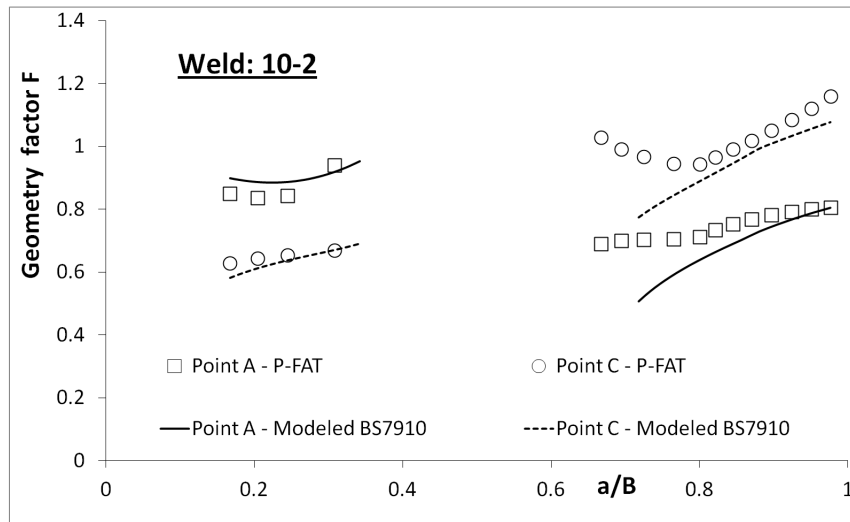


(a)

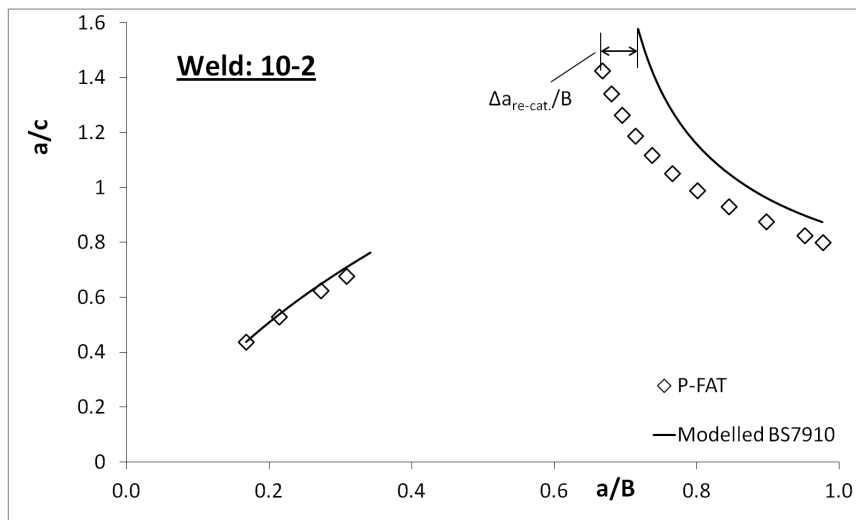


(b)

Figure B.9: Figure a) illustrates the behaviour of the geometry factor in location A and C for weld 9-1 predicted by both P-FAT and the modelled BS7910, while figure b) illustrates the behaviour of the a/c relationship.

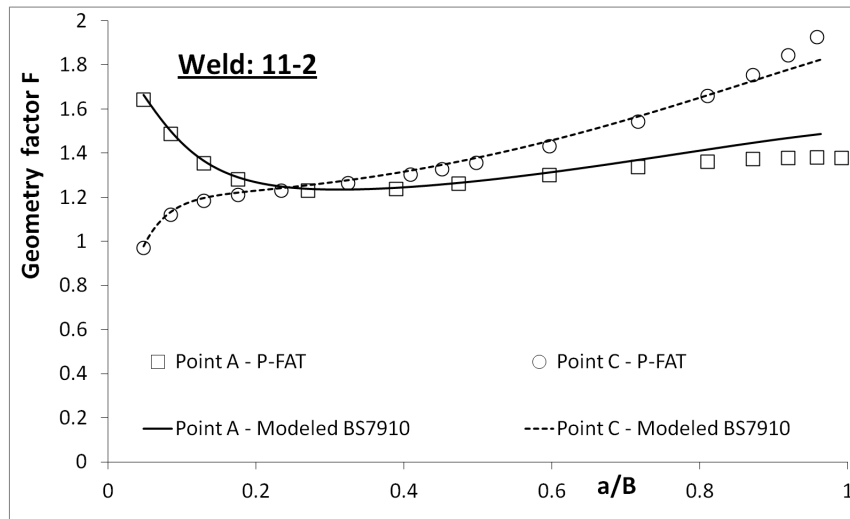


(a)

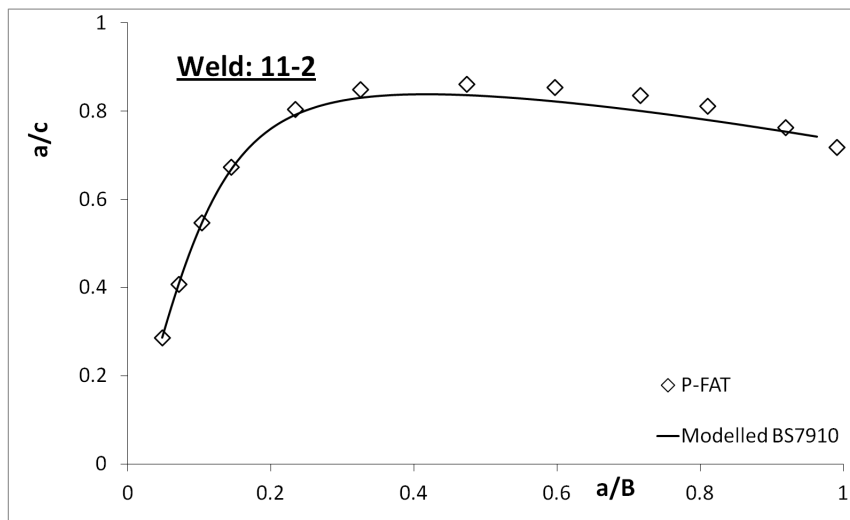


(b)

Figure B.10: Figure a) illustrates the behaviour of the geometry factor in location A and C for weld 1-2 predicted by both P-FAT and the modelled BS7910, while figure b) illustrates the behaviour of the a/c relationship.

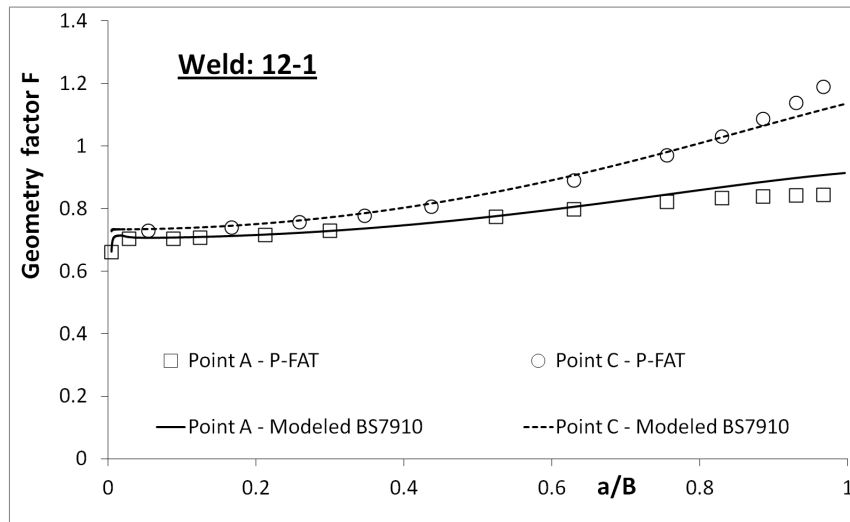


(a)

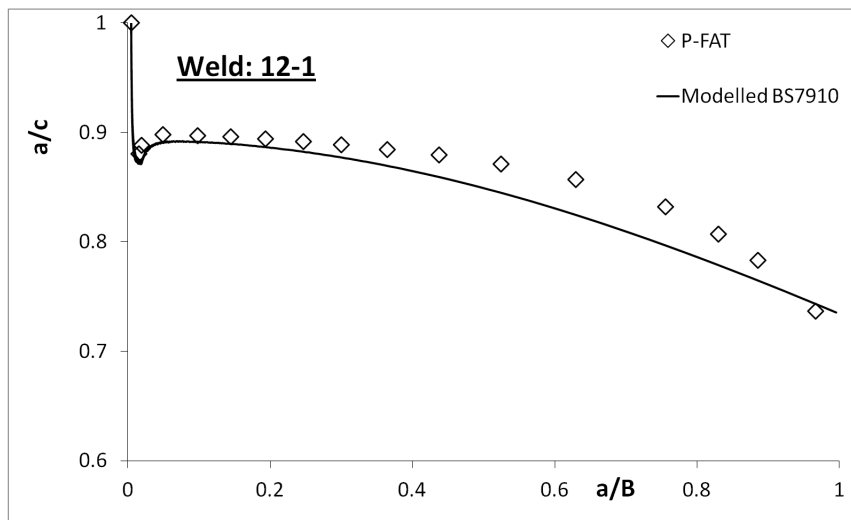


(b)

Figure B.11: Figure a) illustrates the behaviour of the geometry factor in location A and C for weld 11-2 predicted by both P-FAT and the modelled BS7910, while figure b) illustrates the behaviour of the a/c relationship.

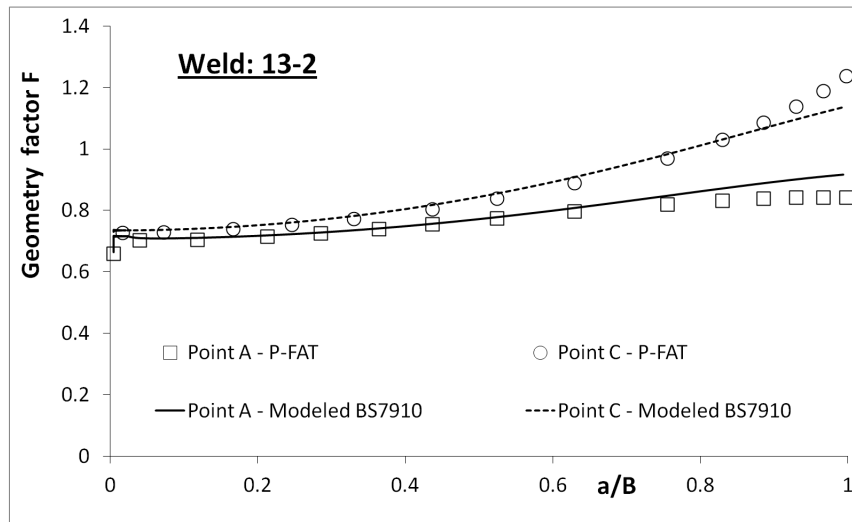


(a)

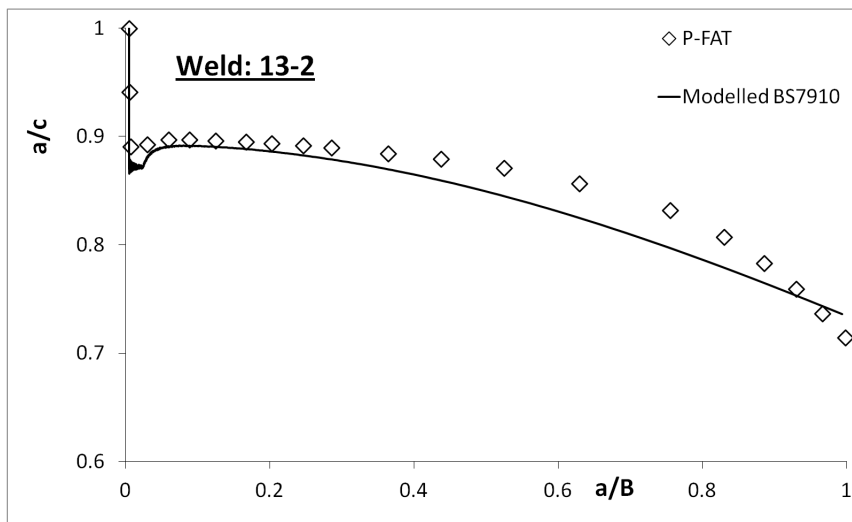


(b)

Figure B.12: Figure a) illustrates the behaviour of the geometry factor in location A and C for weld 12-1 predicted by both P-FAT and the modelled BS7910, while figure b) illustrates the behaviour of the a/c relationship.



(a)



(b)

Figure B.13: Figure a) illustrates the behaviour of the geometry factor in location A and C for weld 1-2 predicted by both P-FAT and the modelled BS7910, while figure b) illustrates the behaviour of the a/c relationship.